

2010

Analysis of the Elastic Field in Functionally Graded Materials

Mohsen Mohammadi

Follow this and additional works at: <https://ir.lib.uwo.ca/digitizedtheses>

Recommended Citation

Mohammadi, Mohsen, "Analysis of the Elastic Field in Functionally Graded Materials" (2010). *Digitized Theses*. 3718.

<https://ir.lib.uwo.ca/digitizedtheses/3718>

This Thesis is brought to you for free and open access by the Digitized Special Collections at Scholarship@Western. It has been accepted for inclusion in Digitized Theses by an authorized administrator of Scholarship@Western. For more information, please contact wlsadmin@uwo.ca.

Analysis of the Elastic Field in Functionally Graded Materials

(Spine title: Elastic Field in FGMs)
(Thesis format: Integrated Article)

by

Mohsen Mohammadi

Faculty of Engineering
Department of Mechanical and Materials Engineering

Submitted in partial fulfillment
of the requirements for the degree of
Doctor of Philosophy

School of Graduate and Postdoctoral Studies
The University of Western Ontario
London, Ontario, Canada

© Mohsen Mohammadi 2010

CERTIFICATE OF EXAMINATION

THE UNIVERSITY OF WESTERN ONTARIO SCHOOL OF GRADUATE AND POSTDOCTORAL STUDIES

Chief Advisor

John R. Dryden

Examining Board

Liying Y. Jiang

Anand V. Singh

Hanping Hong

Craig A. Steeves

The thesis by
Mohsen Mohammadi

entitled

Analysis of the Elastic Field in Functionally Graded Materials

is accepted in partial fulfillment of the
requirements for the degree of
Doctor of Philosophy

Date _____

Chairman of Examining Board

Abstract

In this thesis, the elastic field in circular beams and pipes made of functionally graded materials is considered. The following aspects are presented

First, the thermoelastic stress field in a functionally graded curved beam, where the elastic stiffness varies in the radial direction, is considered. An analytical solution is obtained where the radial variation of the stiffness is represented by a fairly general form. The stress fields corresponding to two different cases for the elastic properties are examined. The flexural stress in the curved beam is then compared with that of a ring. A relatively simple approximate solution is then developed and this is shown to be in good agreement with the analytical results.

Secondly, the effect of a nonconstant Poisson's ratio upon the elastic field in functionally graded axisymmetric solids is analyzed. Both of the elastic coefficients, i.e. Young's modulus and Poisson's ratio, are permitted to vary in the radial direction. These elastic coefficients are considered to be functions of composition and are related on this basis. This allows a closed form solution for the stress function to be obtained. Two cases are discussed in this investigation: a) both Young's modulus and Poisson's ratio are allowed to vary across the radius and the effect of spatial variation of Poisson's ratio upon the maximum radial displacement is investigated; b) Young's modulus is taken as constant and the change in the maximum hoop stress resulting from a variable Poisson's ratio is calculated.

Thirdly, the stress concentration factor around a circular hole in an infinite plate subjected to uniform biaxial tension and pure shear is considered. The plate is made of a functionally graded material where both Young's modulus and Poisson's ratio vary in the radial direction. For plane stress conditions, the governing differential equation for the stress function is derived and solved. A general form for the stress concentration factor in case of biaxial tension is presented. Using a Frobenius series solution, the stress concentration factor is calculated for pure shear case. The stress concentration factor for uniaxial tension is then obtained by superposition of these two modes. The effect of nonhomogeneous stiffness and varying Poisson's ratio upon the stress concentration factors are analyzed. A reasonable approximation in the practical range of Young's modulus is obtained for the stress concentration factor in pure shear loading.

Co-authorship

Professor John R. Dryden is the co-author of the published papers presented in chapters 2 and 3. Professors John R. Dryden and L.Y. Jiang are the co-authors of the accepted paper presented in chapter 4.

Acknowledgements

First of all, I would like to thank my supervisor, Professor John R. Dryden, for his supervision throughout this project. His continuous guidance, technical advice, encouragement, and expertise is greatly appreciated.

I also owe special thanks to my friends and colleagues for their help and friendliness. Their continuous moral support made the completion of this thesis possible.

Finally, I would like to express my sincere gratitude to my family especially my father, mother, and my wife, Zahra (Faezeh) Khatami. Words can not describe your valuable supports during all these years. Without your love, encouragement and patience this would not have been possible.

Contents

CERTIFICATE OF EXAMINATION	ii
ABSTRACT	iii
ACKNOWLEDGEMENTS	v
CONTENTS	vi
LIST OF FIGURES	viii
1 Introduction	1
1.1 Litratione Review	2
1.2 Motivation	4
1.3 Outline of Thesis	5
NOMENCLATURE	1
2 Thermal Stresses in Curved Beams	11
2.1 Introduction	11
2.2 Mathematical formulation of the problem	13
2.2.1 Displacement, strain, and the compatibility condition .	14
2.2.2 Stress and equilibrium	15
2.2.3 Governing differential equation for the stress function .	16
2.3 Method of solution	18
2.3.1 Quantitative results for the elastic field	19
2.4 Curved beam approximation	21
2.5 Results and discussion	23
2.6 Conclusions	26
3 Effect of Varying Poisson's Ratio on Rings	32
3.1 Introduction	32

3.2	Analysis of axisymmetric problems	34
3.2.1	Strain-displacement	35
3.2.2	Hooke's law and equilibrium	36
3.2.3	Relation between E and ν	37
3.3	Governing differential equation	38
3.3.1	Bending problem	39
3.3.2	Spatial variation of elastic properties	39
3.3.3	Solution in the form of hypergeometric functions	40
3.4	Pressurized ring	42
3.4.1	Varying Young's modulus with constant ν_0	42
3.4.2	Constant Young's modulus with varying Poisson's ratio	45
3.5	Discussion and conclusions	48
4	Stress Concentration around a Hole	53
4.1	Introduction	53
4.2	Description of the Inhomogeneity	55
4.3	Governing Differential Equation	56
4.3.1	The general form of the stress function	59
4.4	Stress State due to biaxial Tension: $m = 0$	60
4.4.1	Spatial variation of $\kappa(\rho)$	63
4.5	Stress State due to Pure Shear Loading: $m = 2$	64
4.5.1	Series Solution	65
4.5.2	Solution corresponding to uniform far-field stress	67
4.5.3	Solution associated with $q = -2$	68
4.5.4	Solution associated with $q = 0$	69
4.5.5	The stress function $f(\rho)$ and stress concentration factor K_2	70
4.6	Results and Discussion	72
4.6.1	Effect of nonhomogeneous stiffness upon K_0	73
4.6.2	Effect of nonhomogeneous stiffness upon K_2	75
	Approximate solution	76
4.6.3	Influence of varying Poisson's ratio upon K_0	78
4.6.4	Influence of varying Poisson's ratio upon K_2	79
4.7	Concluding Remarks	81
5	Conclusions and Future Work	87
	VITA	94

List of Figures

2.1	A Curved bar subjected to thermal stress where inner and outer radii are a and b respectively. A dimensionless radius is defined as $\rho = r/a$ and $\beta = b/a$ represents the outer surface.	13
2.2	(a) Dimensionless Young's modulus versus dimensionless radius ρ for $E_1 = E_2$, $\beta = 2$, $s = 2.1$, $m = -5$, and $\gamma = 2.11$; (b) Dimensionless thermal expansion versus dimensionless radius ρ for $A = 1/E$; (c) Dimensionless flexural stress versus dimensionless radius ρ for the curved beam; (d) Dimensionless flexural stress versus dimensionless radius ρ for the ring.	24
2.3	(a) Young's modulus versus dimensionless radius ρ for $E_1 = 68.5\text{GPa}$, $\beta = 3$, $s = -0.002$, $m = 1.34$, and $\gamma = 1.076$; (b) coefficient of thermal expansion versus dimensionless radius ρ for $\alpha_1 = 23.7 \times 10^{-6}\text{K}^{-1}$ and $n = 0.539$; (c) Dimensionless flexural stress versus dimensionless radius ρ for the curved beam; (d) Dimensionless flexural stress versus dimensionless radius ρ	27
3.1	(a) Spatial variation of normalized Young's modulus E/E_α versus dimensionless radius ρ when the constants in equation (3.18) are set as $E_\alpha = E_\beta$, $m = -2$, $\gamma = 0.172$, and $s = 4.1$; (b) Distribution of normalized hoop and radial stresses, S_θ and S_ρ , versus dimensionless radius ρ ; (c) Different spatial variation of Poisson's ratio ν versus dimensionless radius ρ for $\nu_0 = 0.25$; (d) Distributions of corresponding normalized radial displacement u/u_0 versus dimensionless radius ρ	47
3.2	Distributions of exact and approximate maximum normalized hoop stress S versus $\eta = \ln \beta$ for $\omega = \pm 0.5$ and $\omega = 0$. When $\eta < 1/2$, the stress is approximately given by $S \approx 1 + \omega\eta/3$. The maximum and minimum stresses, $S_+ \approx 1.12$ and $S_- \approx 0.88$, differ by about 12% from the case where Poisson's ratio is constant, i.e. $\omega = 0$	49

4.1	Far-field loading on the plate containing the circular hole: a) shows the biaxial loading σ_0 , corresponding to $m = 0$; and b) shows pure shear σ_2 , corresponding to $m = 2$	61
4.2	Graph of normalized Young's modulus $\ln \kappa(\rho)$, defined in equation (4.33), versus dimensionless radius ρ for the values of η and t shown	73
4.3	Graph of $\ln \Sigma_0$ versus t for the values of η shown and Poisson's ratio $\nu_0 = 1/4$. At $t = 0$ the slope is given by equation (4.72). For large values of t the limiting values $\pm 5\eta/8$ are attained . .	74
4.4	Graph of $\ln \Sigma_2$ versus t for the values of η shown and Poisson's ratio $\nu_0 = 1/4$. At $t = 0$ the slope is equal to ϑ which is given by equation (4.74). For large values of t the limiting values $\pm 11\eta/16$ are attained. The solid lines represent the series solution and the dashed lines are obtained from approximation given in equation (4.75)	77
4.5	Graph of $\ln \Sigma_0$ versus t for the values of ω shown. The coefficient $\eta \rightarrow 0$ and Young's modulus is virtually constant; nonetheless, Poisson's ratio varies between ν_1 and ν_∞ . The stress concentration factor differs by 28% from the case where Poisson's ratio is constant	79
4.6	Graph of $\ln \Sigma_2$ versus t for the values of ω shown. The coefficient $\eta \rightarrow 0$ and Young's modulus is virtually constant; nonetheless, Poisson's ratio varies between ν_1 and ν_∞ . The stress concentration factor differs by 13% from the case where Poisson's ratio is constant	81

Nomenclature

r	general radius
ρ	dimensionless radius
θ	angle
a	inner radius
b	outer radius
β	dimensionless outer radius
U	radial displacement
V	tangential displacement
u, u_0	dimensionless radial displacement
v	dimensionless tangential displacement
E, E_1, E_0, E_∞	Young's modulus
E, κ	dimensionless Young's modulus
α, α_1	thermal expansion coefficient
A	dimensionless thermal expansion coefficient
ΔT	temperature change
ϵ_α	thermal strain
ϵ_ρ	radial strain
ϵ_θ	tangential strain
$\gamma_{\rho\theta}$	shear strain
σ_ρ	radial stress
σ_θ	tangential stress
$\sigma_{\rho\theta}$	shear stress
S_ρ	normalized radial stress
S_θ	normalized tangential stress
$\sigma_0, \sigma_1, \sigma_2$	reference stress
p, f, ψ, ϕ	stress function
$\nu, \nu_1, \nu_\infty, \omega$	Poisson's ratio
g, h	effect of inhomogeneity
$G(\rho, \theta)$	Green's function
$p_1, p_2, f_1, f_2, f_3, f_4$	general solution
$M(a, b, x)$	Kummer's function
ϵ_f	flexural strain
S_f	normalized flexural stress
P_1, P_2	Legendre polynomials
P	internal pressure
K_0, K_2, K	stress concentration factor
Σ_0, Σ_2	normalized stress concentration factor

Chapter 1

Introduction

The concept of functionally graded materials (FGMs) was first initiated as a means of preparing thermal barrier materials in 1984 in Sendai, Japan [1]. Since then, functionally graded materials have received significant consideration see e.g. [2, 3].

FGMs possess a number of advantages that make them attractive, including a potential reduction of in-plane and transverse through-the-thickness stresses, an improved residual stress distribution, enhanced thermal properties, higher fracture toughness, and enhanced stress intensity factors [4]. These inhomogeneous solids are now used in different branches of engineering applications, e.g. dental implants [5], fuel cells [6], and energy applications [7].

FGMs are nonhomogeneous composites, which consist of two or more phases. The most common FGMs are metal/ceramic composites, where the ceramic part has a good thermal resisting properties and the metal has superior fracture toughness. The composition and the morphology of FGMs gradually change over the volume; consequently, the elastic properties of the material change with position [8]. This can be used to produce desirable stress

and strain fields. Of particular interest in this contribution is the special case where the elastic properties within a body vary in the radial direction but are independent of tangential direction. This type of inhomogeneity can be due to several causes: directional cooling leading to a microstructural gradient [9]; phase segregation arising as a result of centrifugal casting [10]; property degradation of the fuel cladding in nuclear reactors [11]; chemical and vapor deposition [12]; and surface modification using laser technology [13, 14]. The change in elastic properties of such kind of inhomogeneity has been studied experimentally for different materials recently [15].

In recent years, the stress field caused by pressure and (or) temperature variation acting on pipes, rings, and plates made of functionally graded materials has been discussed several times by scientists and engineers [16, 17, 18]. Similarly some investigation have been also done on examining the stress field induced by mechanical loads such as bending in circular curved bar [19, 20]. However, the problem of thermoelastic stress field in non-homogeneous curved beams has not received much attention.

1.1 Literature Review

Boley and Barrekette [21] investigated the thermoelastic stresses in homogeneous curved beams under temperature varying in the radial direction. They compared the solution obtained from the theory of elasticity with an approximate solution based on the strength of materials. In addition, some investigations dealing with thermal stresses in nonhomogeneous anisotropic solid cylinders and curved beams have been done [22, 23, 24, 25]. In these works, the cylinder was considered to be fixed in one end and the temperature variation was defined with polynomials in axial direction. Subsequently, Mohammadi

and Dryden [26] discussed the problem of thermal stresses in a functionally graded curved beam. In their contribution Young's modulus and thermal expansion changed only in the radial direction and obeyed a power law function so that, the properties are either monotonically decreasing or increasing in the radial direction.

In most of the investigations on elastic analysis of FGMs only Young's modulus has been considered to vary with position and Poisson's ratio is taken as being constant. This simplifies the analysis. However, experimental measurements indicate that Poisson's ratio is not constant in FGMs, see e.g. [27]. The change in Poisson's ratio affects the elastic field.

Lutz and Zimmerman [28, 29] analyzed thermal stresses in functionally graded spherical and cylindrical vessels due to the uniform heating. In their contribution, λ and μ , i.e. two Lamè's elastic coefficients, were considered to vary across the radius. Paulino and Kim [30] showed that Poisson's ratio was an important factor on the fracture of FGMs and it could have significant influence on the stress intensity factor and T-stress of a crack under a mixed-mode loading condition. Recently, Eraslan [31] has analyzed a FG pressurized tube under non-uniform temperature distribution. Young's modulus, Poisson's ratio, and thermal expansion were considered to vary with position according to a power law. The governing differential equation was solved numerically.

There has been less analytical investigation on the effect of radial inhomogeneity upon the elastic field in non-axisymmetric problems, see e.g. [32, 33]. Curved beams have been investigated by Lekhnitskii [16]. Other geometries such as hollow cylinders by Shao et al. [34], spheres by Poultangari et al. [35], pressurized vessels by Jabbari et al. [36], and spherical inclusions by Lutz and Zimmerman [37]. In most of these contributions power law functions have been used to define the variation of elastic properties. Here we want to calculate

the stress field around a circular hole subjected to uniform far-field stress and power law functions are not suitable to define the spatial variation of Young's modulus in an infinite plate.

The stress concentration factor around a hole in a homogeneous plate has received much attention over the last decades see e.g. [38, 39]. In the case of functionally graded materials, some numerical work has been done recently. Using an isoparametric finite element formulation, Kubair and Bhanu-Chandar [40] investigated stress concentration around a circular hole in functionally graded panels under uniaxial tension. They found that the stress concentration factor was reduced when Young's modulus progressively decreases towards the hole. Subsequently, Yang et al. [41] investigated the stress field around a circular hole in a FGM plate. They used piece-wise homogeneous layers and complex variable methods. The plate was decomposed into N rings with equal thickness and constant material properties. The elastic fields for different spatial variations of the elastic properties were calculated.

1.2 Motivation

In this thesis, using the fundamental theory of mathematical elasticity, the elastic field in functionally graded materials is investigated. Curved beams, pipes, and rings are of particular interest; thus, polar coordinates are used to formulate the problems. Both elastic and thermal properties are considered to vary across the radius. A fairly general form, i.e. exponential function, is used to define the material's inhomogeneity. Here, both axisymmetric and nonaxisymmetric problems of elasticity are considered. It is considered that the material is linear elastic and obeys Hooke's law.

1.3 Outline of Thesis

The remainder of the thesis is laid out as follows:

1. Chapter 2 presents an analysis to find the thermal stress in a curved beam and a ring made of a functionally graded materials .
2. Chapter 3 considers the influence of nonconstant Poisson's ratio upon the elastic deformation in FGMs.
3. Chapter 4 gives an analytical calculation for the stress concentration factor around a circular hole (due to uniform far-field tension) in an infinite FG plate.
4. Chapter 5 presents some general conclusions and suggests future work.

Chapters 2, 3, and 4 are reprints of papers that have been published or accepted.

Bibliography

- [1] M. Koizumi. FGM activities in Japan. *Composites Part B*, 28B:1–4, 1997.
- [2] C.O. Horgan and A.M. Chan. The pressurized hollow cylinder or disk problem for functionally graded isotropic linearly elastic materials. *Journal of Elasticity*, 55:pp. 43–59, 1999.
- [3] M. Jabbari, S. Sohrabpour, and M.R. Eslami. Mechanical and thermal stresses in a functionally graded hollow cylinder due to radially symmetric loads. *International Journal of Pressure Vessels and Piping*, 79:493–497, 2002.

- [4] V. Birman and L.W. Byrd. Modeling and analysis of functionally graded materials and structure. *Applied Mechanics Reviews*, 60:195–216, 2007.
- [5] F. Watari, A. Yokoyama, F. Saso, M. Uo, and T. Kawasaki. Fabrication and properties of functionally graded dental implant. *Composites Part B*, 28:pp. 5–11, 1997.
- [6] J. Simonet, G. Kapelski, and D. Bouvard. A sedimentation process for the fabrication of solid oxide fuel cell cathodes with graded composition. *Journal of the European Ceramic Society*, 27:3113–3116, 2007.
- [7] E. Muller, C. Draar, J. Schilz, and W.A. Kaysser. Functionally graded materials for sensor and energy applications. *Materials Science and Engineering A*, 362:17–39, 2003.
- [8] Y. Miyamoto, W.A. Kaysser, R.H. Rabin, A. Kawasaki, and R.G. Ford. *Functionally Graded Materials: Design, Processing and Applications*. Kluwer Academic Publishers, USA, 1999.
- [9] A.J. Markworth, K.S. Ramesh, and W.P. Parks. Modelling studies applied to functionally graded materials. *Journal of Materials Science*, 30:2183–2193, 1995.
- [10] Y. Fukui, N. Yamanaka, and K. Wakashima. The stresses and strains in a thick-walled tube for functionally graded material under uniform thermal loading. *JSME International Journal A-Solid Mechanics*, 36:156–162, 1993.
- [11] G. Subbaraman and K.L. Reifsnider. Mechanical response of fuel clad with radial property variations. In 12th Annual. Mtg. Ses., volume 36, pages 1235–1247, University of Texas, 1976.

- [12] L.B. Freund and S. Suresh. *Thin Film Materials*. Cambridge University Press, Cambridge, 2003.
- [13] M. Picasso, C.F. Marsden, J.D. Wagniere, A. Frenk, and M. Rappaz. A simple but realistic model for laser cladding. *Metallurgical and Materials Transactions B*, 25:281–291, 1994.
- [14] M.U. Islam. An overview of research in the fields of laser surface modification and laser machining at the integrated manufacturing technologies institute NRC. *Advanced Performance Materials*, 3:215–238, 1996.
- [15] M.S. Ozmusul and R.C. Picu. Elastic moduli of particulate composites with graded filler-matrix interface. *Polymer Composites*, 23:110–119, 2002.
- [16] S.G. Lekhnitskii. *Theory of Elasticity of an Anisotropic Body*. Mir Publishers, Moscow, 1981.
- [17] N. Noda. Thermal stresses in functionally graded materials. *Journal of Thermal Stresses*, 22:477–512, 1999.
- [18] N. Tutuncu and M. Ozturk. Exact solutions for stresses in functionally graded pressure vessels. *Composites Part B: Engineering*, 32:493–497, 2001.
- [19] G.A. Kardomateas. Bending of a cylindrically orthotropic curved beam with linearly distributed elastic constants. *The Quarterly Journal of Mechanics and Applied Mathematics*, 43:43–56, 1990.
- [20] J.R. Dryden. Bending of inhomogeneous curved bars. *International Journal of Solids and Structures*, 44:4158–4166, 2007.

- [21] B.A. Boley and E.S. Barrekette. Thermal stress in curved beams. *J. Aero. Space. Sci.*, 25:627–630, p. 643, 1958.
- [22] D. Iesan. On the thermal stresses in beams. *J. Eng. Math.*, 6:155–163, 1972.
- [23] S. Chirita. Thermal stresses in anisotropic cylinders. *Acta Mech.*, vol. 23:301–306, 1975.
- [24] D. Iesan. Thermal stresses in composite cylinders. *J. Therm. Stresses*, 3:495–508, 1980.
- [25] S. Chirita. Thermal stresses in anisotropic noncylindrical beams. *Rev. Roum. Sci. Techn-Mec. Appl.*, 28:63–74, 1983.
- [26] M. Mohammadi and J.R. Dryden. Thermal stress in a functionally graded curved bar. In *The Proceedings of Simulation and Modeling (MS 2007)*, pages 250–253, Montreal, Quebec, Canada, 2007.
- [27] P.R. Marur and H.V. Tippur. Evaluation of mechanical properties of functionally graded materials. *Journal of Testing and Evaluation*, 26:539–545, 1998.
- [28] R.W. Zimmerman and M.P. Lutz. Thermal stresses and thermal expansion in a uniformly heated functionally graded cylinder. *Journal of Thermal Stresses*, 22:177–188, 1999.
- [29] M.P. Lutz and R.W. Zimmerman. Thermal stresses and effective thermal expansion coefficient of a functionally gradient sphere. *Journal of Thermal Stresses*, 19:39–54, 1996.

- [30] G.H. Paulino and J-H. Kim. On the poisson's ratio effect on mixed-mode stress intensity factors and t-stress in functionally graded materials. *International Journal of Computational Engineering Science*, 5:833–861, 2004.
- [31] A.N. Eraslan. Stresses in FGM pressure tubes under non-uniform temperature distribution. *Structural Engineering and Mechanics*, 26:393–408, 2006.
- [32] G.J. Nie and R.C. Batra. Static deformations of functionally graded polar-orthotropic cylinders with elliptical inner and circular outer surfaces. *Composites Science and Technology*, doi:10.1016/j.compscitech.2009.11.018, 2009.
- [33] R.C. Batra and G.J. Nie. Analytical solutions for functionally graded incompressible eccentric and non-axisymmetrically loaded circular cylinders. *Composite Structures*, doi:10.1016/j.compstruct.2009.10.022, 2009.
- [34] Z. S. Shao, K. K. Ang, J. N. Reddy, and T. J. Wang. Nonaxisymmetric thermomechanical analysis of functionally graded hollow cylinders. *Journal of Thermal Stresses*, 31:pp. 515–536, 2008.
- [35] R. Poultangari, M. Jabbari, and M.R. Eslami. Functionally graded hollow spheres under non-axisymmetric thermo-mechanical loads. *International Journal of Pressure Vessels and Piping*, 85:295–305, 2008.
- [36] M. Jabbari, S. Sohrabpour, and M.R. Eslami. General solutions for mechanical and thermal stresses in a functionally graded hollow cylinder due to nonaxisymmetric steady-state loads. *Journal of Applied Mechanics Transactions of ASME*, 70:pp. 111–118, 2003.

- [37] M.P. Lutz and R.W. Zimmerman. Effect of the interphase zone on the bulk modulus of a particulate composite. *Journal of Applied Mechanics Transactions of ASME*, 63:855–861, 1996.
- [38] G.N. Savin. *Stress Concentration around Holes*. International Series of Monographs in Aeronautics and Astronautics. Pergamon Press, New York, 1961.
- [39] W.D. Pilkey and D.F. Pilkey. *Peterson's Stress Concentration Factors*. John Wiley and Sons INC., Hoboken, New Jersey, third edition, 2008.
- [40] D.V. Kubair and B. Bhanu-Chandar. Stress concentration factor due to a circular hole in functionally graded panels under uniaxial tension. *International Journal of Mechanical Sciences*, 50:pp. 732–742, 2008.
- [41] Q. Yang, C.-F. Gao, and W. Chen. Stress analysis of a functional graded material plate with a circular hole. *Archive of Applied Mechanics*, July 2009.

Chapter 2

Thermal Stresses in Curved Beams

2.1 Introduction

The¹ concept of functionally graded materials (FGMs) was first proposed as a means of preparing thermal barrier materials in 1984 [1]. Since then, functionally graded materials have received a significant amount of scientific consideration and these inhomogeneous solids have been used in different engineering applications. It is noted that, the properties of these solids can be tailored. In these composites both the composition and the structure gradually change over the volume, resulting in corresponding changes in the properties of the material to produce a desirable elastic field [2]. Of particular interest in this contribution is the special case where the elastic properties within a curved beam vary in the radial direction but are independent of θ . This type of inhomogeneity can be due to several causes: directional cooling leading to a

¹M. Mohammadi and J. R. Dryden, Thermal Stress in a Nonhomogeneous Curved Beam, Journal of Thermal Stresses, Vol. 31. No.6, June. 2008, 1-12.

microstructural gradient [3]; phase segregation arising as a result of centrifugal casting [4]; property degradation of the fuel cladding in nuclear reactors [5]; chemical and vapor deposition [6]; and surface modification using laser technology [7, 8].

In recent years, the stress field caused by pressure and (or) temperature variation acting on pipes, rings, and plates made of functionally graded materials has been discussed several times by scientists and engineers [9, 10, 11, 12, 13]. Similarly some investigation have been also done on examining the stress field induced by mechanical loads such as bending in circular curved bar [9, 14, 15]. However, the problem of thermoelastic stress field in non-homogeneous curved beams has not received much attention.

Boley and Barrekette [16] investigated the thermoelastic stresses in homogeneous curved beams under temperature varying in the radial direction. They compared the solution obtained from the theory of elasticity with an approximate solution based on the strength of materials. In addition, some investigations dealing with thermal stresses in nonhomogeneous anisotropic solid cylinders and curved beams were done [18, 19]. In these works, the cylinder was considered to be fixed in one end and the temperature variation was defined with polynomials in axial direction. Subsequently, Mohammadi and Dryden [21] discussed the problem of thermal stresses in functionally graded curved beam. In their contribution Young's modulus and coefficient of thermal expansion changed only in the radial direction and obeyed a power law function so that, the properties are either monotonically decreasing or increasing in the radial direction. A slightly more general form will be used here to define Young's modulus and coefficient of thermal expansion. Poisson's ratio is considered as a constant in this investigation and this has been shown not to be a serious deficiency [11, 22].

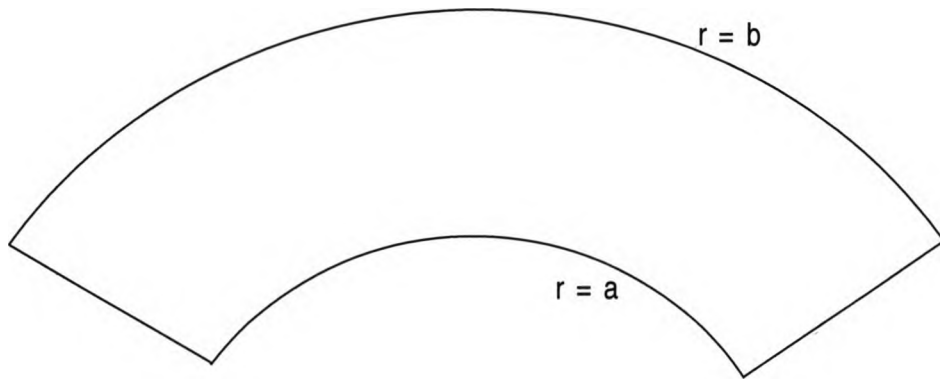


Figure 2.1: A Curved bar subjected to thermal stress where inner and outer radii are a and b respectively. A dimensionless radius is defined as $\rho = r/a$ and $\beta = b/a$ represents the outer surface.

In Section 2.5, two different cases for the spatial variation of Young's modulus and coefficient of thermal expansion are investigated. In the first case the elastic properties are defined symmetrically which roughly corresponds to a coating on outer surfaces of the beam. In the second case the elastic properties obtained from experimental tests [23] are used to calculate the stress field. The analytical solution is then compared with an approximate model based on strength of materials. Finally, the thermoelastic flexural stress field in a ring is compared with that of a curved beam.

2.2 Mathematical formulation of the problem

The curved beam illustrated in Fig. 2.1 is bounded by inner radius a and outer radius b . The cross section of the beam is rectangular and has unit depth. A dimensionless variable $\rho = r/a$ in the radial direction is defined so that the inner and outer surfaces are $\rho = 1$ and $\rho = \beta = b/a$ respectively. In addition,

dimensionless displacements $u = U/a$ and $v = V/a$ are defined. Both Young's modulus and thermal expansion are considered to vary in the radial direction so that, $E(\rho)$ and $\alpha(\rho)$ can be written as

$$E \equiv E_1 E(\rho), \quad \alpha \equiv \alpha_1 A(\rho), \quad (2.1)$$

where E_1 and α_1 are the properties at $\rho = 1$ of the curved beam. The dimensionless functions E and A describe the radial variation of Young's modulus and coefficient of thermal expansion respectively. Now suppose that the stress free temperature is T_0 and the beam is subjected to a uniform temperature change ΔT , so that the thermal strain ϵ_α is defined as

$$\epsilon_\alpha = \epsilon_1 A(\rho), \quad (2.2)$$

where $\epsilon_1 = \alpha_1 \Delta T$ is constant. The aim here is to find the stress field induced by this nonuniform thermal strain.

2.2.1 Displacement, strain, and the compatibility condition

The curved beam is considered to be in plane stress and the average values of displacement, strain, and stress across the thickness are used [24]. For the sake of simplicity the overbar is omitted from all of these average values.

Apart from the rigid body modes, the displacement that leads to strain is given by

$$u = u_0(\rho) + \int \epsilon_\alpha d\rho, \quad (2.3)$$

$$v = B\rho\theta. \quad (2.4)$$

The strain-displacement equations in polar coordinates are well known, see for example [25], and they are as below

$$\epsilon_\rho = \frac{du_0}{d\rho} + \epsilon_\alpha, \quad (2.5)$$

$$\epsilon_\theta = \frac{u_0}{\rho} + \frac{1}{\rho} \int \epsilon_\alpha d\rho + B, \quad (2.6)$$

and the shear strain, $\epsilon_{\rho\theta} = 0$. It follows that the compatibility condition is written as

$$\frac{d(\rho\epsilon_\theta)}{d\rho} - \epsilon_\rho = B \quad (2.7)$$

Boley and Weiner [26] discussed the case when the solid is homogeneous while here the effect of inhomogeneity is investigated.

2.2.2 Stress and equilibrium

Under conditions of plane stress, the Hooke's law is expressed as

$$\epsilon_\rho = \frac{\sigma_\rho - \nu\sigma_\theta}{E} + \epsilon_\alpha, \quad (2.8)$$

$$\epsilon_\theta = \frac{\sigma_\theta - \nu\sigma_\rho}{E} + \epsilon_\alpha. \quad (2.9)$$

In passing it is noted that in plane strain case E, ν and ϵ_α are replaced by $E/(1 - \nu^2)$, $\nu/(1 - \nu)$, and $(1 + \nu)\epsilon_\alpha$ respectively. Upon inspection of the Hooke's law, it is seen that the stresses are proportional to $\sigma_1 = E_1\epsilon_1$. There-

fore, normalized radial and tangential stresses are defined as follows

$$S_\rho = \frac{\sigma_\rho}{\sigma_1}, \quad S_\theta = \frac{\sigma_\theta}{\sigma_1}.$$

Mechanical equilibrium in both axial and tangential directions is identically satisfied and the condition for radial equilibrium is

$$\frac{d(\rho S_\rho)}{d\rho} = S_\theta. \quad (2.10)$$

A stress function, $p = p(\rho)$, which depends solely upon the radial variables is used. The stresses are then defined by

$$S_\rho = \frac{p}{\rho}, \quad S_\theta = \frac{dp}{d\rho} \quad (2.11)$$

and with this definition the radial equilibrium is identically satisfied.

2.2.3 Governing differential equation for the stress function

The main goal of this chapter is to examine the role of nonhomogeneous stiffness upon the thermoelastic stress field. It has been shown that [11, 22] Poisson's ratio does not generally influence the stress and moreover setting ν equal to a constant leads to a significant simplification in the analysis. So upon substituting equation (2.11) into Hooke's law (2.8-2.9) and putting the resultant strains into the compatibility equation (2.7), an ordinary differential equation is obtained which is written as

$$\left(\frac{\rho p'}{E}\right)' - \left(\frac{1-\nu g}{\rho E}\right)p = \Delta M - \rho A', \quad (2.12)$$

where $\Delta M = B/\epsilon_1$ and it is equal to zero for a ring. If the ring is cut, a curved beam is created and if the ends of this beam are free of stress, it follows that the total moment must vanish. The quantity ΔM is then found from the condition $\int_a^b r\sigma_\theta dr = 0$. Thus, there is no moment applied to the beam. The function g contains the effect of inhomogeneity and is defined by

$$g = \frac{\rho E'}{E}. \quad (2.13)$$

The surface is stress free, i.e. $S_\rho(1) = S_\rho(\beta) = 0$, and hence the boundary conditions for equation (2.12) are specified as follows

$$p(1) = 0, \quad (2.14)$$

$$p(\beta) = 0. \quad (2.15)$$

In addition, the moment applied to the curved beam is equal to zero, so that the dimensionless moment $M = \int_1^\beta \rho S_\theta d\rho = \int_1^\beta \rho p' d\rho = 0$, and the third boundary condition is written as

$$\int_1^\beta p(\rho) d\rho = 0, \quad (2.16)$$

which is obtained by using integration by parts and this determines ΔM . It is necessary to solve the differential equation (2.12) with the boundary conditions given by equations (2.14-2.16). Across the end of the beam the stress σ_θ is not equal to zero in this treatment, however, since both the flexural resultant and the moment vanish, it follows by St. Venant's principle, i.e. softening the boundary conditions [27], that the solution is reasonable at small distances

from the end of the curved beam.

2.3 Method of solution

Suppose that $p_1(\rho)$ and $p_2(\rho)$ are two linearly independent solutions of the homogeneous equation

$$\left(\frac{\rho p'}{E}\right)' - \left(\frac{1-\nu g}{\rho E}\right)p = 0. \quad (2.17)$$

It is possible then to obtain a solution of the nonhomogeneous equation (2.12) by constructing the Green's function; this method is described in standard textbooks, e.g. [28, 29]. The functions $\psi_1(\rho)$ and $\psi_2(\rho)$ are linear combinations of $p_1(\rho)$ and $p_2(\rho)$ that are given by

$$\begin{aligned} \psi_1(\rho) &= \frac{p_1(1)p_2(\rho) - p_2(1)p_1(\rho)}{p_1'(1)p_2(1) - p_2'(1)p_1(1)}, \\ \psi_2(\rho) &= \frac{p_1(\beta)p_2(\rho) - p_2(\beta)p_1(\rho)}{p_1(\beta)p_2(1) - p_2(\beta)p_1(1)}. \end{aligned} \quad (2.18)$$

Note that the functions $\psi_1(\rho)$ and $\psi_2(\rho)$ satisfy the homogeneous boundary conditions $\psi_1(1) = \psi_2(\beta) = 0$. The Green's function $G(\rho, \xi)$ is then defined as

$$G(\rho, \xi) = -[\psi_2(\xi)\psi_1(\rho)H(\xi - \rho) + \psi_1(\xi)\psi_2(\rho)H(\rho - \xi)],$$

where $H(x)$ is Heaviside function and ξ lies in the interval $1 < \xi < \beta$. The solution to equation (2.12) in terms of Green's function is then written as

$$p(\rho) = \Delta M \int_1^\beta G(\rho, \xi) d\xi - \int_1^\beta \xi A'(\xi) G(\rho, \xi) d\xi. \quad (2.19)$$

This stress function satisfies the governing differential equation (2.12) along with the three boundary conditions given in equations (2.14 -2.16). The constant ΔM is adjusted so that $\int_1^\beta p d\rho = 0$ and hence the moment vanishes. The coefficient ΔM for the curved beam can then be found as

$$\Delta M = \frac{\int_1^\beta \int_1^\beta \xi A'(\xi) G(\rho, \xi) d\xi d\rho}{\int_1^\beta \int_1^\beta G(\rho, \xi) d\xi d\rho}. \quad (2.20)$$

If ΔM is equal to zero, the differential equation converts to the problem of a ring where there is only displacement in the radial direction and the moment across the wall thickness is not equal to zero.

2.3.1 Quantitative results for the elastic field

To obtain quantitative results the spatial distribution of $E(\rho)$ and $A(\rho)$ needs to be specified. Mohammadi and Dryden [21] solved the equation for the case when both Young's modulus and thermal expansion obey a power law. It is obvious that the properties defined by the power law are either monotonically increasing or decreasing. A slightly more general form for Young's modulus has been introduced by [30] and $E(\rho)$ is then written as

$$E(\rho) = \rho^{2m} \exp[\gamma(\rho^s - 1)], \quad (2.21)$$

where m , γ , and s are real constants. If E_1 and E_2 are the values of Young's modulus at the inner and outer surfaces of the curved beam respectively, then γ is obtained as

$$\gamma = \frac{\ln E_2 - \ln E_1 - 2m \ln \beta}{\beta^s - 1}.$$

Inserting the expression for E into equation (2.13) leads to $g = 2m + s\gamma\rho^s$, and equation (2.17) becomes

$$\rho^2 \frac{d^2 p}{d\rho^2} + (1 - 2m - s\gamma\rho^s)\rho \frac{dp}{d\rho} - (1 - 2m\nu - s\nu\gamma\rho^s)p = 0. \quad (2.22)$$

This can be transformed into Kummer's equation, and the solution to the homogeneous differential equation (2.22) can be obtained [15]. The two linearly independent solutions are

$$p_1(\rho) = \rho^{\zeta_1} M(a_1, b_1, \gamma\rho^s),$$

$$p_2(\rho) = \rho^{\zeta_2} M(a_2, b_2, \gamma\rho^s),$$

where $M(a, b, x)$ is Kummer's function and the constants are defined as follows:

$$\zeta_1 = m + \kappa, \quad \zeta_2 = m - \kappa,$$

$$a_1 = (\zeta_1 - \nu)/s, \quad a_2 = (\zeta_2 - \nu)/s,$$

$$b_1 = (s + 2\kappa)/s, \quad b_2 = (s - 2\kappa)/s,$$

where κ is positive and $\kappa = \sqrt{1 - 2m\nu + m^2}$. The properties of Kummer's function can be found in various mathematical references, e.g. [31, 32]. Putting $p_1(\rho)$ and $p_2(\rho)$ into the expression for the Green's function, the solution to the governing differential equation is obtained.

2.4 Curved beam approximation

It is useful to compare the results of the elastic solution with those of an approximate model based on the curved beam theory that appears in elementary strength of materials. In this theory, the elastic radial displacement is considered as constant and the effect of Poisson's ratio is neglected. Boley and Barrekette [16] discussed this problem for constant Young's modulus and thermal expansion due to non-uniform temperature difference. According to the standard beam treatment, the dimensionless elastic flexural stress in the direction parallel to the axis of the beam is written as

$$S_f = E(\rho) [\epsilon_f - A], \quad (2.23)$$

where ϵ_f and S_f are the flexural strain and stress respectively and as usual in this type of approximation the Poisson effect is neglected. In the curved beam treatment the term u_0 in equation (2.3) is regarded as being a constant and the tangential displacement is given in equation (2.4) so that the cross sections remain plane. Using equation (2.6), the total strain in the flexural direction is found and the dimensionless stress is

$$S_f = E(\rho) \left[\frac{u_0}{\rho} + B + \frac{1}{\rho} \int A d\rho - A \right]. \quad (2.24)$$

The two boundary conditions representing the situation that no force or moment is applied to the beam are then stated as

$$\int_1^\beta S_f d\rho = 0, \quad (2.25)$$

$$\int_1^\beta S_f \rho d\rho = 0, \quad (2.26)$$

These conditions give the constants u_0 and B . It is noted that for a ring there is no tangential displacement so that $B = 0$ and the second boundary condition, equation (2.26), is not necessarily satisfied. If Young's modulus has the form given in equation (2.21) then integrals of the type

$$\int_0^\rho z^{n-1} e^{\gamma z^s} dz = \frac{\rho^n}{n} M\left(\frac{n}{s}, 1 + \frac{n}{s}, \gamma \rho^s\right) \quad (2.27)$$

are required to evaluate the boundary conditions.

It is convenient to write A and E in terms of series involving Legendre polynomials [31]. The dimensionless functions A and E are then written as

$$A = A_0 + A_1 P_1(y) + A_2 P_2(y) + \dots, \quad (2.28)$$

$$E = E_0 + E_1 P_1(y) + E_2 P_2(y) + \dots,$$

where $y = (\rho - \rho_c)/h$, $\rho_c = (\beta + 1)/2$ is the centroid of the beam, and $2h = \beta - 1$.

The coefficients are given by

$$A_n = \frac{2n + 1}{2} \int_{-1}^1 A(y) P_n(y) dy, \quad (2.29)$$

$$E_n = \frac{2n + 1}{2} \int_{-1}^1 E(y) P_n(y) dy.$$

The two coefficients u_0 and B are then found by evaluating the simpler inte-

grals

$$\int_{-1}^1 S_f dy = 0, \quad (2.30)$$

$$\int_{-1}^1 S_f y dy = 0, \quad (2.31)$$

With regard to the terms $A_0 + A_1 P_1(y)$ in equation (2.28), the quantity A_0 represents stress free expansion, while the term $A_1 P_1(y)$ leads to a stress of order h^2 . In comparison, these two terms cause no stress in a straight beam.

2.5 Results and discussion

It is noted that in both equations (2.12) and (2.24) a thermal expansion of the form $\alpha = \alpha_1 + \alpha_2 \ln \rho$, leads to no stress in the beam. However, this form causes stress in the ring. Here, two cases are examined where the thermoelastic stress field is non-zero. The first case deals with the thermoelastic stress field in a curved beam with coating on both surfaces. In the second case, elastic properties obtained from experimental data are used and the corresponding flexural stress field is obtained.

In the first case, suppose that the dimensions of the beam are such that $\beta = 2$ and Fig. 2.2(a) shows the spatial variation of dimensionless Young's modulus which is symmetric across the radius of the curved beam. Roughly speaking this represents a coating when the same material is diffused into each surface of the curved beam, so that $E_1 = E_2$. The parameters m , s , and γ

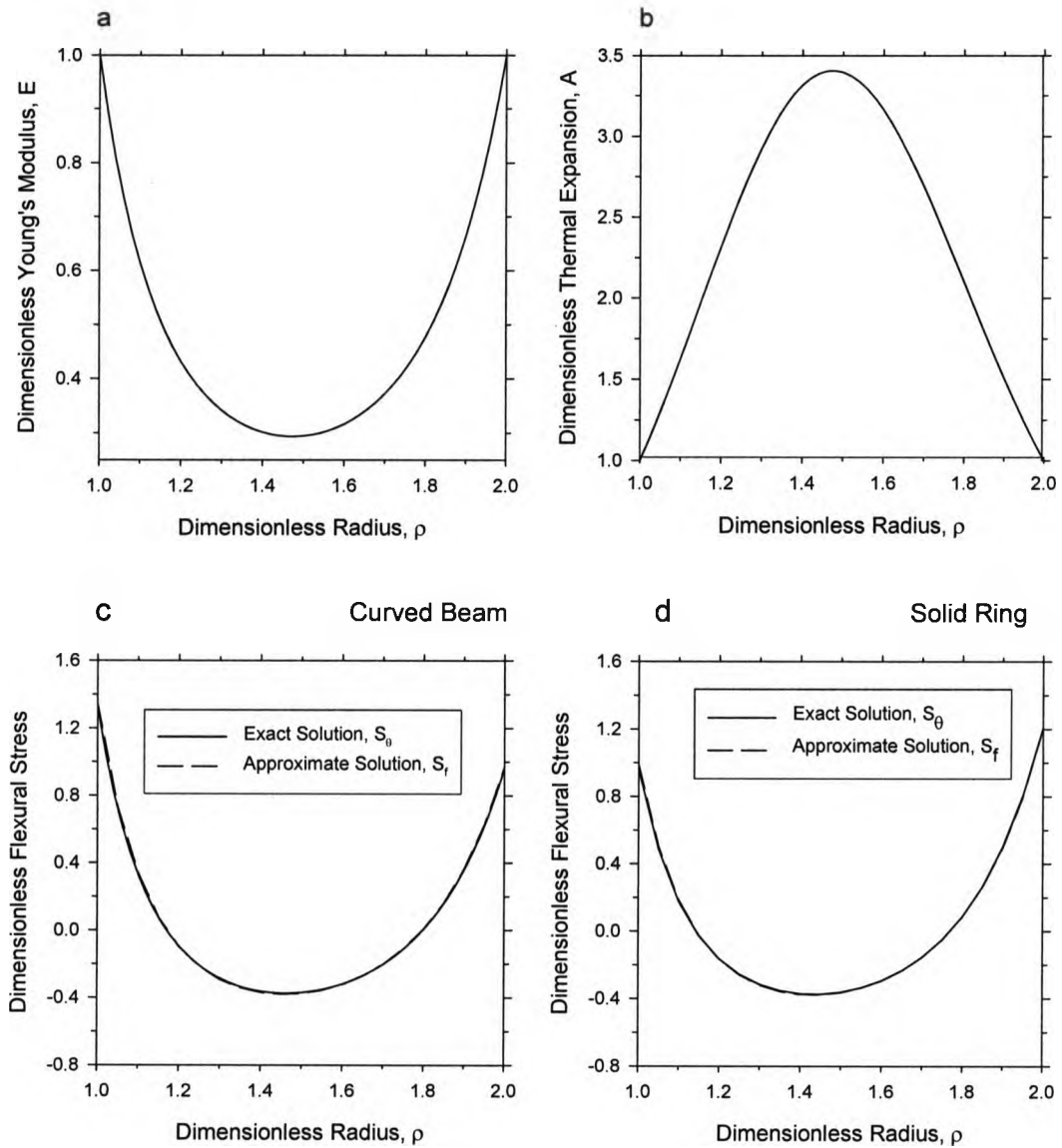


Figure 2.2: (a) Dimensionless Young's modulus versus dimensionless radius ρ for $E_1 = E_2$, $\beta = 2$, $s = 2.1$, $m = -5$, and $\gamma = 2.11$; (b) Dimensionless thermal expansion versus dimensionless radius ρ for $A = 1/E$; (c) Dimensionless flexural stress versus dimensionless radius ρ for the curved beam; (d) Dimensionless flexural stress versus dimensionless radius ρ for the ring.

are found so that Young's modulus is symmetric with respect to the centroid of the beam: $m = -5$ and $s = 2.1$. To have a symmetrical distribution for coefficient of thermal expansion as well as Young's modulus the thermal expansion is made reciprocal to Young's modulus; there is some justification by this assumption [33]. The spatial distribution of dimensionless thermal expansion is shown in Fig. 2.2(b). Using six series terms for E and A gives results that are virtually indistinguishable from those shown in Figs. 2.2(a, b). The stress field is almost independent of Poisson's ratio and here $\nu = 1/3$. Fig. 2.2(c) shows the distribution of S_θ in the curved beam. The result of S_f is also illustrated. Evidently, the elasticity solution is in good agreement with the approximate solution. The radial stress field is small in comparison with the flexural stress and is not shown. Now, the major difference in the stress field between a ring and a curved beam arises from the fact that in the latter the net moment across the section is completely relaxed. In view of the material symmetry shown in Figs. 2.2(a) and 2.2(b), it is expected that the moment in a ring is likely to be small, and, indeed the flexural stress in a ring, which is illustrated in Fig. 2.2(d), does not differ very much from the curved beam.

In the second case, the elastic properties of an aluminum-based centrifugally cast FGM are considered. These properties are obtained from experimental analysis [23]. The geometry of the curved beam is such that $\beta = 1.25$. The expression for E given in equation (2.21), is fitted to the experimental data and this is shown in Fig. 2.3(a). The various parameters used are $m = 1.34$, $s = -0.002$, $\gamma = 1.076$, and $E_1 = 68.5$ GPa. The experimental results suggest that the coefficient of thermal expansion is a decreasing function of Young's modulus and to model this behavior we assume that $\alpha \approx \rho^{2n}/E$. Thus, the

dimensionless coefficient of thermal expansion $A(\rho)$ is written as

$$A(\rho) = \rho^{2(n-m)} \exp[\gamma(1 - \rho^s)], \quad (2.32)$$

where n is equal to a real constant. This expression is adjusted to fit the experimental data by setting $n = 0.539$ and $\alpha_1 = 23.7 \times 10^{-6} \text{K}^{-1}$ as shown in Fig. 2.3(b). Using two series terms for E and A gives results that are virtually indistinguishable from those shown in Figs. 2.3(a, b). The stresses S_θ and S_f corresponding to a curved beam are illustrated in Fig. 2.3(c). In comparison, Fig. 2.3(d) shows the behavior of these stresses in a ring. Clearly the stress is much greater in the ring and this is due to the fact that there is an unrelaxed bending moment across the wall.

2.6 Conclusions

The reasonably general form given in equation (2.21) for the spatial distribution of dimensionless Young's modulus has been used. Two different cases for the spatial distribution of elastic properties were investigated. In the first case the Young's modulus and the coefficient of thermal expansion were considered to change symmetrically across the radius representing coatings on inner and outer radii of the beam. Thermoelastic stress field in the coated curved beam and a coated ring as a special case were then calculated. Because of the material symmetry, a small net bending moment was induced in the ring and hence, the flexural stress was almost the same as in the beam. In the second case the analytical functions for the elastic properties were fitted to the obtained experimental data. Then the distribution of flexural stress was investigated in the curved beam and the ring. The material properties are not symmetrical

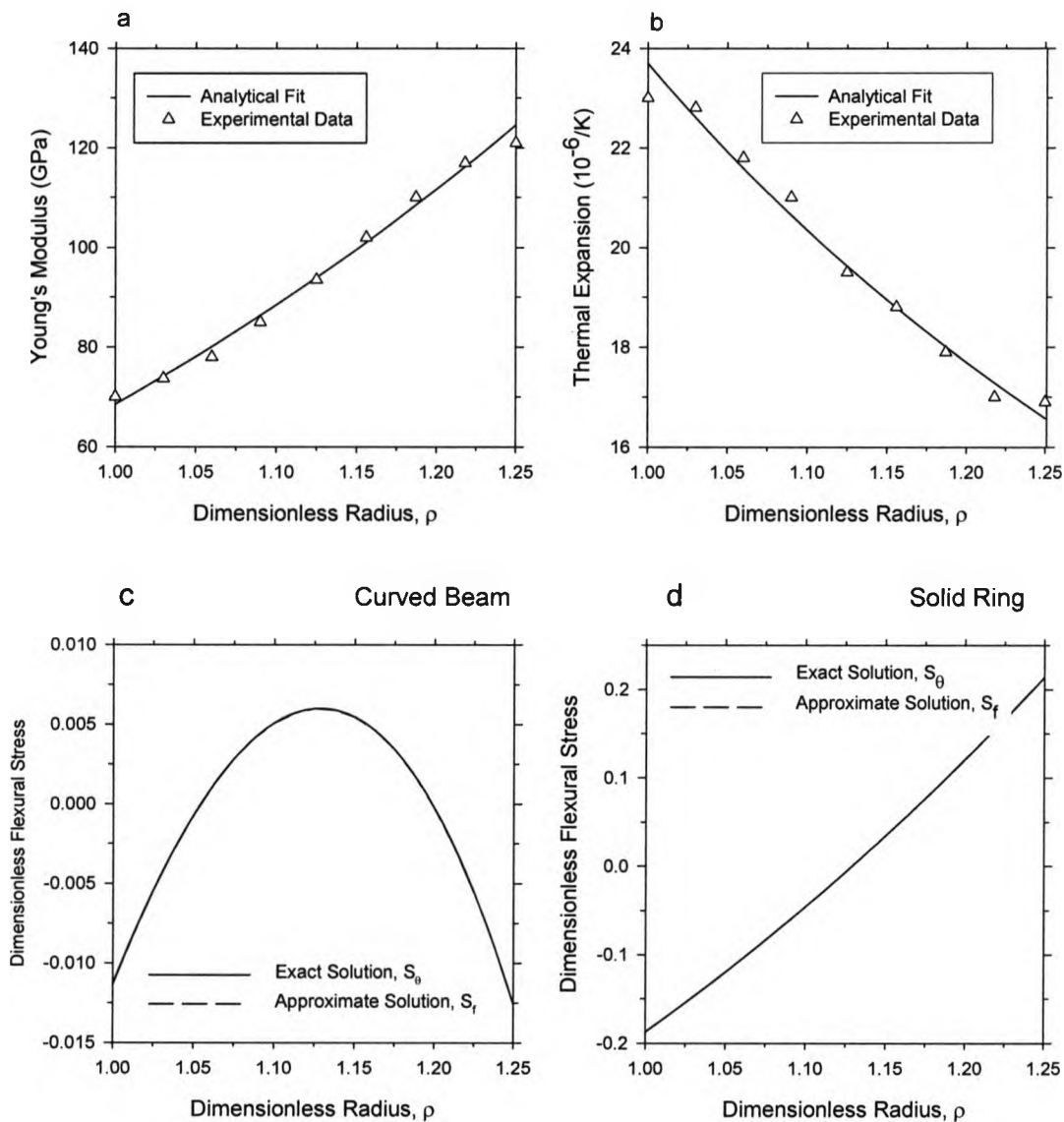


Figure 2.3: (a) Young's modulus versus dimensionless radius ρ for $E_1 = 68.5\text{GPa}$, $\beta = 3$, $s = -0.002$, $m = 1.34$, and $\gamma = 1.076$; (b) coefficient of thermal expansion versus dimensionless radius ρ for $\alpha_1 = 23.7 \times 10^{-6}\text{K}^{-1}$ and $n = 0.539$; (c) Dimensionless flexural stress versus dimensionless radius ρ for the curved beam; (d) Dimensionless flexural stress versus dimensionless radius ρ .

across the beam so that unlike the previous case, ΔM is large. Consequently, the stress in the ring is high in comparison with the beam. It is noted that, in all cases good agreement was observed between the analytical solution, S_θ , and the approximate solution, S_f .

Bibliography

- [1] M. Koizumi. FGM activities in Japan. *Composites Part B*, 28B:1–4, 1997.
- [2] Y. Miyamoto, W.A. Kaysser, R.H. Rabin, A. Kawasaki, and R.G. Ford. *Functionally Graded Materials: Design, Processing and Applications*. Kluwer Academic Publishers, USA, 1999.
- [3] A.J. Markworth, K.S. Ramesh, and W.P. Parks. Modelling studies applied to functionally graded materials. *Journal of Materials Science*, 30:2183–2193, 1995.
- [4] Y. Fukui, N. Yamanaka, and K. Wakashima. The stresses and strains in a thick-walled tube for functionally graded material under uniform thermal loading. *JSME International Journal A-Solid Mechanics*, 36:156–162, 1993.
- [5] G. Subbaraman and K.L. Reifsnider. Mechanical response of fuel clad with radial property variations. In 12th Annual. Mtg. Ses., volume 36, pages 1235–1247, University of Texas, 1976.
- [6] L.B. Freund and S. Suresh. *Thin Film Materials*. Cambridge University Press, Cambridge, 2003.
- [7] M. Picasso, C.F. Marsden, J.D. Wagniere, A. Frenk, and M. Rappaz. A

- simple but realistic model for laser cladding. *Metallurgical and Materials Transactions B*, 25:281–291, 1994.
- [8] M.U. Islam. An overview of research in the fields of laser surface modification and laser machining at the integrated manufacturing technologies institute NRC. *Advanced Performance Materials*, 3:215–238, 1996.
- [9] S.G. Lekhnitskii. *Theory of Elasticity of an Anisotropic Body*. Mir Publishers, Moscow, 1981.
- [10] N. Noda. Thermal stresses in functionally graded materials. *Journal of Thermal Stresses*, 22:477–512, 1999.
- [11] C.O. Horgan and A.M. Chan. The pressurized hollow cylinder or disk problem for functionally graded isotropic linearly elastic materials. *Journal of Elasticity*, 55:pp. 43–59, 1999.
- [12] N. Tutuncu and M. Ozturk. Exact solutions for stresses in functionally graded pressure vessels. *Composites Part B: Engineering*, 32:493–497, 2001.
- [13] M. Jabbari, S. Sohrabpour, and M.R. Eslami. Mechanical and thermal stresses in a functionally graded hollow cylinder due to radially symmetric loads. *International Journal of Pressure Vessels and Piping*, 79:493–497, 2002.
- [14] G.A. Kardomateas. Bending of a cylindrically orthotropic curved beam with linearly distributed elastic constants. *The Quarterly Journal of Mechanics and Applied Mathematics*, 43:43–56, 1990.
- [15] J.R. Dryden. Bending of inhomogeneous curved bars. *International Journal of Solids and Structures*, 44:4158–4166, 2007.

- [16] B.A. Boley and E.S. Barrekette. Thermal stress in curved beams. *J. Aero. Space. Sci.*, 25:627–630, p. 643, 1958.
- [17] D. Iesan. On the thermal stresses in beams. *J. Eng. Math.*, 6:155–163, 1972.
- [18] S. Chirita. Thermal stresses in anisotropic cylinders. *Acta Mech.*, vol. 23:301–306, 1975.
- [19] D. Iesan. Thermal stresses in composite cylinders. *J. Therm. Stresses*, 3:495–508, 1980.
- [20] S. Chirita. Thermal stresses in anisotropic noncylindrical beams. *Rev. Roum. Sci. Techn-Mec. Appl.*, 28:63–74, 1983.
- [21] M. Mohammadi and J.R. Dryden. Thermal stress in a functionally graded curved bar. In *The Proceedings of Simulation and Modeling (MS 2007)*, pages 250–253, Montreal, Quebec, Canada, 2007.
- [22] B. Paul. Prediction of elastic constants of multiphase materials. *Transactions of the Metallurgical Society-AIME*, 218:36–41, 1960.
- [23] Y. Watanabe and Y. Fukui. Fabrication of aluminum based functionally graded materials by centrifugal method and their physical properties. *Light Metals*, vol. 46:pp. 395–403, 1996.
- [24] A.E.H. Love. *A Treatise on the Mathematical Theory of Elasticity*. Cambridge University Press Warehouse, second edition, 1906.
- [25] S. Timoshenko and J.N. Goodier. *Theory of Elasticity*. McGraw-Hill, New York, third edition, 1970.

Chapter 3

Effect of Varying Poisson's Ratio on Rings

3.1 Introduction

Functionally¹ graded materials (FGMs) are nonhomogeneous composites, which consist of two or more phases. The most common FGMs are metal/ceramic composites, where the ceramic part has a good thermal resisting properties and the metal has superior fracture toughness. These inhomogeneous solids are used in different branches of engineering applications, e.g. transport systems, energy conversion and cutting tools [1, 2]. FGMs possess a number of advantages that make them attractive, including a potential reduction of in-plane and transverse through-the-thickness stresses, an improved residual stress distribution, enhanced thermal properties, higher fracture toughness, and enhanced stress intensity factors [3]. The composition and the morphol-

¹M. Mohammadi and J. R. Dryden, Influence of the Spatial Variation of Poissons Ratio upon the Elastic Field in Nonhomogeneous Axisymmetric Bodies, *International Journal of Solids and Structures*, Vol. 46. Nos 3&4, February 2009, 788-795.

ogy of FGMs gradually change over the volume; consequently, the elastic properties of the material change with position [2]. This can be used to produce desirable stress and strain fields.

Of particular interest in this contribution is the special case where the elastic properties within an axisymmetric body vary in the radial direction but are independent of tangential direction. This type of inhomogeneity can be due to several causes: directional cooling leading to a microstructural gradient [4]; phase segregation arising as a result of centrifugal casting [5]; and surface modification using laser technology [6, 7]. The change in elastic properties of such kind of inhomogeneity has been studied experimentally for different materials recently [5, 8].

Scientists and engineers have investigated the stress and displacement fields caused by pressure and (or) temperature variation acting on pipes, vessels, and plates made of functionally graded materials in polar coordinates [9, 10]. Less analysis has been done on examining the stress field induced by mechanical and thermal loads in circular curved bars see e.g. [11, 12]. In these investigations only Young's modulus has been considered to vary with position and Poisson's ratio is taken as being constant. This simplifies the analysis.

However, experimental measurements indicate that Poisson's ratio is not constant in FGMs, see e.g. [13]. The change in Poisson's ratio affects the elastic field. Lutz and Zimmerman [14, 15] analyzed thermal stresses in functionally graded spherical and cylindrical vessels due to the uniform heating. In their contribution, λ and μ , i.e. two Lamè's elastic coefficients, were considered to vary across the radius. Paulino and Kim [16] showed that Poisson's ratio was an important factor on the fracture of FGMs and it could have significant influence on the stress intensity factor and T-stress of a crack under a mixed-mode loading condition. Recently, Eraslan [17] has analyzed a FG pressurized

tube under non-uniform temperature distribution. Young's modulus, Poisson's ratio, and thermal expansion were considered to vary with position according to a power law. The governing differential equation was solved numerically.

Here, the general formulation of the elastic stress field for axisymmetric problems in polar coordinates is obtained. In this contribution both Young's modulus and Poisson's ratio are considered to vary across the radius. Using the law of mixtures, Young's modulus and Poisson's ratio are related and a closed form solution for the stress function in terms of hypergeometric functions is obtained. This investigation is focused on the effect of spatial variation of Poisson's ratio upon the maximum radial displacement and maximum normalized hoop stress for a pressurized tube.

3.2 Analysis of axisymmetric problems

To begin, the general governing differential equation for axisymmetric deformations is derived and then this equation with special boundary conditions is solved for a ring. In the cylindrical coordinates the inner and outer radii are equal to a and b respectively. This deformable body is made of a functionally graded material whose elastic properties only change across the radius. It is convenient to use normalized variables. The dimensionless radius is $\rho = r/a$ so that the inner and outer surfaces are $\rho = \alpha = 1$ and $\rho = \beta = b/a$ respectively. In addition, dimensionless displacements $u = U/a$ and $v = V/a$ are defined. Young's modulus, E and Poisson's ratio, ν are considered to vary in the radial direction. The aim here is to find the effect of these nonhomogeneities especially, radially dependent Poisson's ratio on the stress field. To begin the analysis, let us start with the strain-displacement relations.

3.2.1 Strain-displacement

Suppose that the elastic body is in a condition of plane stress, where $\sigma_z = 0$. In polar coordinate the average values of displacement, strain, and stress across the thickness are used [18]. For the sake of simplicity the overbar is omitted from all of these average values. The strain-displacement equations in polar coordinates for axisymmetric bodies are familiar, see for example [19], and they are written as

$$\epsilon_\rho = \frac{du}{d\rho}, \quad (3.1)$$

$$\epsilon_\theta = \frac{u}{\rho} + B, \quad (3.2)$$

$$\epsilon_{\rho\theta} = 0, \quad (3.3)$$

where $u = u(\rho)$ and B is an unknown constant. Aside from the terms containing the rigid body translation and rotations, the displacement field can be written as

$$u = u(\rho), \quad (3.4)$$

$$v = B\rho\theta. \quad (3.5)$$

The constant B is equal to zero for a ring; otherwise, the displacement is not single-valued. Using these equations, it follows that the compatibility condition is written as

$$\frac{d(\rho\epsilon_\theta)}{d\rho} - \epsilon_\rho = B. \quad (3.6)$$

In 1852 Lamè studied the problem of elastic stresses in pressurized homogeneous cylindrical pipes. About thirty years later, Golovin and Ribière independently investigated the stress field due to the bending in a curved beam made of a homogeneous material [19].

3.2.2 Hooke's law and equilibrium

In plane stress, Hooke's law for an isotropic nonhomogeneous elastic body is expressed as

$$\epsilon_\rho = \frac{\sigma_\rho - \nu\sigma_\theta}{E}, \quad (3.7)$$

$$\epsilon_\theta = \frac{\sigma_\theta - \nu\sigma_\rho}{E}. \quad (3.8)$$

It is noted that for the plane strain case E and ν are replaced by $E/(1 - \nu^2)$ and $\nu/(1 - \nu)$ respectively. In the axisymmetric problem assumed here, mechanical equilibrium in both axial and tangential directions is identically satisfied and the condition for the radial equilibrium is [19]

$$\frac{d(\rho\sigma_\rho)}{d\rho} = \sigma_\theta. \quad (3.9)$$

A stress function, $\phi = \phi(\rho)$, which depends solely upon the radial variables is used. The stresses are then defined by

$$\sigma_\rho = \frac{\phi}{\rho}, \quad \sigma_\theta = \frac{d\phi}{d\rho} \quad (3.10)$$

and with this definition the radial equilibrium is identically satisfied.

3.2.3 Relation between E and ν

Generally, it is acknowledged that Young's modulus and Poisson's ratio are independent quantities. However, in functionally graded materials the composition C varies with radial position, and the elastic properties here are taken as being functions of composition, i.e. $E = f_1(C)$ and $\nu = f_2(C)$, where the influence of structural morphology is neglected. In this type of treatment, both E and ν attain an extremum when $dC/dr = 0$ and are constant when C is uniform. If it is possible to invert these equations so that $C = f_1^{-1}(E) = f_2^{-1}(\nu)$, then this will provide a relationship between E and ν . A simple, albeit crude, approximation that captures these features is to use the law of mixtures so that

$$E \approx \alpha_0 + \alpha_1 C, \quad (3.11)$$

$$\nu \approx \beta_0 + \beta_1 C. \quad (3.12)$$

Upon solving for C in equation(3.11) it follows that $\nu \approx \gamma_0 + \gamma_1 E$ where γ_0 and γ_1 are the appropriate constants which can be either positive or negative. Since the concentration varies with ρ , it follows that Young's modulus can be written as

$$E = E_0 \zeta, \quad (3.13)$$

where ζ is a dimensionless function of ρ describing the spatial variation of Young's modulus and E_0 has appropriate units. The expression for Poisson's ratio then has the form

$$\nu \approx \nu_0 + \nu_1 \zeta, \quad (3.14)$$

where the constants ν_0 and ν_1 can be adjusted to provide the best fit for the radial profile of Poisson's ratio. It is noted that a FGM which has a constant Poisson's ratio, i.e. $\nu = \nu_0$, corresponds to the case where $\nu_1 = 0$.

3.3 Governing differential equation

To obtain the governing differential equation, which the stress function must satisfy, the following steps are undertaken. First, the results in equation (3.10) are substituted into Hooke's law to give the strain in terms of the stress function. Secondly, these strains are inserted into the compatibility equation (3.6). Finally, using the relationship between Young's modulus and Poisson's ratio, given in equation (3.14), the differential equation that emerges is written as

$$\frac{d^2\phi}{d\rho^2} + \frac{d\phi}{d\rho} \left\{ \frac{1-g}{\rho} \right\} - \phi \left\{ \frac{1-\nu_0 g}{\rho^2} \right\} = \frac{EB}{\rho}. \quad (3.15)$$

where the function g contains the effect of nonhomogeneous stiffness and is given by [11]

$$g = \frac{\rho}{E} \frac{dE}{d\rho}. \quad (3.16)$$

The governing differential equation (3.15) does not have any dependence upon ν_1 so that the stress function ϕ depends only upon g and ν_0 . Hence the stress field can be viewed as pertaining to a solid having a constant Poisson's ratio equal to ν_0 and whose the spatial variation of E is described by the function g .

3.3.1 Bending problem

Suppose that $\phi_1(\rho)$ and $\phi_2(\rho)$ are the two complementary solutions to equation (3.15) and as stated above these solutions depend upon ν_0 and g . Using standard results from the theory of ordinary differential equations, see for instance [20], it can be shown that with appropriate scaling the Wronskian of $\phi_1(\rho)$ and $\phi_2(\rho)$ is equal to E/ρ . It then follows that the particular solution $\chi(\rho)$ to equation (3.15) has the form

$$\chi(\rho) = B \int_1^{\rho} [\phi_2(\rho)\phi_1(t) - \phi_1(\rho)\phi_2(t)] dt. \quad (3.17)$$

The coefficient B depends upon the stress field and is chosen so that the bending moment is equal to a specified value; consequently, B is insensitive to the coefficient ν_1 . Therefore, unlike the radial displacement, the tangential displacement, $v = B\rho\theta$, has no dependence whatsoever upon ν_1 . Since the purpose of this note is to consider the influence of the spatial variation of Poisson's ratio, only the pressurized ring problem, where there is solely radial displacement, is considered in this contribution.

3.3.2 Spatial variation of elastic properties

Young's modulus in equation (3.13) is defined by the relation $E = E_0\zeta$ and the function ζ needs to be defined. A power law, i.e. $\zeta = \rho^m$, is commonly used to define the spatial distribution of elastic and thermal properties, (see for example [10]). The two parameters E_0 and m can be adjusted to approximate the radial behavior of Young's modulus. It is noted that the power law is either an increasing or decreasing function depending on the sign of the exponent so that its usefulness is restricted to FGMs whose Young's modulus has this

shape. Moreover, the form $E = E_0\rho^{2m}$ can not be used to solve either the exterior problem corresponding to a hole in an infinite plate which includes the region $\rho \rightarrow \infty$, or the interior problem corresponding to a solid disk which includes the region $\rho \rightarrow 0$.

For these reasons a slightly more general expression to define the radial distribution of Young's modulus has been proposed [21]

$$E = E_a\rho^{2m} \exp[\gamma(\rho^s - 1)], \tag{3.18}$$

where m , γ , and s are real constants and E_a is the value of Young's modulus at $r = a$. This expression has four adjustable parameters; thus, it has more flexibility in modeling the shape of the stiffness profile than does the power law. For either the interior or the exterior problem, the coefficient $m = 0$ so that $E = E_0 \exp(\gamma\rho^s)$ and the appropriate sign for s is used.

3.3.3 Solution in the form of hypergeometric functions

Inserting the expression for $E = E_0\zeta$ into equation (3.16) leads to $g = 2m + s\gamma\rho^s$; thus, the homogeneous part of equation (3.15) becomes

$$\rho^2 \frac{d^2\phi}{d\rho^2} + (1 - 2m - s\gamma\rho^s)\rho \frac{d\phi}{d\rho} - (1 - 2m\nu_0 - s\nu_0\gamma\rho^s)\phi = 0. \tag{3.19}$$

Consider ϕ_1 and ϕ_2 as two linearly independent solution of equation (3.19). The first solution is $\phi_1 = \rho_1^{n_1}y_1$. By substituting this into the differential equation, it is found that y_1 is a solution of

$$\rho^2 \frac{d^2y_1}{d\rho^2} + (1 + 2\kappa - s\gamma\rho^s)\rho \frac{dy_1}{d\rho} - s\gamma\rho^s(n_1 - \nu_0)y_1 = 0.$$

The constants are defined later. Now, on setting $z = \gamma\rho^s$, it follows that y_1 satisfies the Kummer's equation [11] and it is written as

$$z \frac{d^2 y_1}{dz^2} + (b_1 - z) \frac{dy_1}{dz} - a_1 y_1 = 0.$$

The solution to Kummer's differential equation is Kummer's or confluent hypergeometric function $M(a_1, b_1; z)$. Thus, ϕ_1 can be attained. It is noted that ϕ_2 is obtained by the same procedure and the two linearly independent solutions to equation (3.19) are [11, 12]

$$\phi_1(\rho) = \rho^{n_1} M(a_1, b_1, \gamma\rho^s), \quad (3.20)$$

$$\phi_2(\rho) = \rho^{n_2} M(a_2, b_2, \gamma\rho^s), \quad (3.21)$$

where the constants are defined as follows

$$\begin{aligned} n_1 &= m + \kappa, & n_2 &= m - \kappa, \\ a_1 &= \frac{n_1 - \nu_0}{s}, & a_2 &= \frac{n_2 - \nu_0}{s}, \\ b_1 &= \frac{s + 2\kappa}{s}, & b_2 &= \frac{s - 2\kappa}{s}, \end{aligned}$$

where $\kappa \equiv \sqrt{1 - 2m\nu_0 + m^2}$. The properties of Kummer's function are familiar [22]. Kummer's function is defined as

$$M(a, b, z) = \sum_{n=0}^{\infty} \frac{(a)_n z^n}{(b)_n n!},$$

where $(a)_n$ is Pochhammer notation and it is written as

$$(a)_n = a(a+1)(a+2)\dots(a+n-1).$$

More properties of this function can be found in mathematical references, e.g. [22].

3.4 Pressurized ring

An internally pressurized functionally graded ring has inner and outer radii equal to $\alpha = 1$ and $\rho = \beta = b/a$ respectively so that both solutions, $\phi_1(\rho)$ and $\phi_2(\rho)$, are needed. The ring is subjected to an internal pressure P , causing the boundary conditions for this problem as

$$\sigma_\rho(1) = -P, \quad \implies \quad \phi(1) = -P, \quad (3.22)$$

$$\sigma_\rho(\beta) = 0, \quad \implies \quad \phi(\beta) = 0. \quad (3.23)$$

Upon solving equation (3.19) with the boundary conditions (3.22-3.23), the solution for the stress function can be written as

$$\phi = P \left[\frac{\phi_2(\beta)\phi_1(\rho) - \phi_2(\rho)\phi_1(\beta)}{\phi_2(1)\phi_1(\beta) - \phi_2(\beta)\phi_1(1)} \right]. \quad (3.24)$$

where $\phi(1) = -P$ and $\phi(\beta) = 0$.

3.4.1 Varying Young's modulus with constant ν_0

As previously stated, the stresses do not depend upon ν_1 and are completely specified for given values of g and ν_0 . The purpose of this section is to illustrate the effect of ν_1 upon the displacement u for a given function g . To begin, consider a pressurized ring where $\beta = 2$ and the spatial variation of Young's

modulus is adjusted so that $E_a = E_b$. The constants in equation (3.18) can be adjusted in various ways to produce this condition and here $m = -2$, $\gamma = 0.172$, and $s = 4.1$. The function ζ is then approximately given by

$$\zeta \approx \frac{\exp [0.172 (\rho^{4.10} - 1)]}{\rho^4}. \quad (3.25)$$

The graph of $\zeta = E/E_a$ is shown in Fig. 3.1(a) and the function $g = (d\zeta/d\rho)\rho/\zeta$. A material of this type, where the properties are almost symmetrical with respect to the middle surface $c = (a + b)/2$, can arise due to diffusion in the radial direction from each surface. In the limiting case, if m and s are made very large, the stiffness profile approximates thin coatings on the inner and outer surfaces. If $\nu_a = \nu_b$ are the boundary values for Poisson's ratio then according to equation (3.14) ν is written as

$$\nu = \nu_0 + (\nu_a - \nu_0)\zeta \quad (3.26)$$

and due to symmetry $\nu_1 = \nu_a - \nu_0$. The constant ν_0 is arbitrary and here $\nu_0 = 0.25$. Normalized stress components can be introduced which are specified as below

$$\begin{aligned} S_\rho &= \frac{\sigma_\rho}{\sigma_0}, \\ S_\theta &= \frac{\sigma_\theta}{\sigma_0}, \end{aligned} \quad (3.27)$$

where $\sigma_0 = P/(\beta - 1)$ is the average hoop stress. The distribution of dimensionless stress components S_ρ and S_θ corresponding to $\nu_0 = 0.25$ is shown in Fig. 3.1(b).

Although the spatial variation of ν does not affect the stress, it does have an influence upon the displacement. Using Hooke's Law, $E\epsilon_\theta = \sigma_\theta - \nu\sigma_\rho$, the displacement u is found as

$$u = \frac{\rho}{E}(\sigma_\theta - \nu\sigma_\rho). \quad (3.28)$$

To show the influence of ν upon displacement, the following two cases are considered:

Case (1): The coefficients $\nu_0 = 0.25$, $\nu_a = 0$;

Case (2): The coefficients $\nu_0 = 0.25$, $\nu_a = 0.5$.

These are shown in Fig. 3.1(c) along with constant Poisson's ratio $\nu = \nu_0 = 0.25$. The displacement corresponding to these cases is shown in Fig. 3.1(d) and the results in this figure can be explained by considering equation (3.28). The maximum displacement, u_a occurs at the inner surface $\rho = 1$ and according to Fig. 3.1(b), the quantities $\sigma_\theta \approx 2.75P$ and $\sigma_\rho = -P$. The displacement u_a can then be written as

$$u_a \approx \frac{P(2.75 + \nu_a)}{E_a}. \quad (3.29)$$

The displacements in Fig. 3.1(d) are normalized with respect to $u_0 \approx 3P/E_a$ corresponding to material having constant Poisson's ratio $\nu = \nu_a = \nu_0 = 0.25$. As can be seen in the figure u_a varies by about 15% between cases (1) and (2). At the outer surface $\rho = 2$, the radial stress $\sigma_\rho = 0$ and according to equation (3.28) the displacement is the same for all cases.

3.4.2 Constant Young's modulus with varying Poisson's ratio

The purpose of this section is to investigate the stresses in a pipe where Young's modulus is constant and Poisson's ratio changes from ν_a to ν_b across the wall thickness. To begin, it is well known that if both Poisson's ratio and Young's modulus are constant, the maximum stress in the hoop direction, $\sigma_0 = P(\beta^2 + 1)/(\beta^2 - 1)$, occurs at the inner surface and can be rewritten

$$\sigma_0 = \frac{P}{\tanh \eta}, \quad (3.30)$$

where $\eta = \ln \beta$ and $\tanh \eta = (e^{2\eta} - 1)/(e^{2\eta} + 1)$. Since we want to examine the effect of the spatial variation of Poisson's ratio upon σ_0 , a case where Young's modulus is virtually constant is considered. On the other hand, Poisson's ratio is allowed to change across the thickness from ν_a to ν_b . To achieve this condition, we set

$$E = E_a \rho^{2m}, \quad (3.31)$$

and perform a limiting process where $m \rightarrow 0$. The governing differential equation (3.19) becomes

$$\rho^2 \frac{d^2 \phi}{d\rho^2} + \rho \frac{d\phi}{d\rho} - (1 - 2m\nu_0)\phi = 0. \quad (3.32)$$

According to equations (3.14) and (3.31), Poisson's ratio is given by the form $\nu = \nu_0 + \nu_1 \rho^{2m}$ where the coefficients are adjusted to satisfy ν_a and ν_b at the end points. As $m \rightarrow 0$ it is expected that ν_0 becomes infinite and indeed it

follows after some algebra that

$$\nu_0 = \frac{\beta^{2m}\nu_a - \nu_b}{\beta^{2m} - 1} \sim \frac{\nu_a - \nu_b}{2m \ln \beta}. \quad (3.33)$$

The quantity $-2m\nu_0$ then becomes

$$-2m\nu_0 \approx \frac{\omega}{\eta}, \quad (3.34)$$

where $\omega = \nu_b - \nu_a$ and $\eta = \ln \beta$. The expression for Poisson's ratio becomes

$$\nu \approx \nu_a + \omega \left\{ \frac{\ln \rho}{\ln \beta} \right\} \quad (3.35)$$

So the material here has constant Young's modulus and Poisson's ratio changes monotonically across the wall thickness.

The reduced differential equation (3.32) is an Euler-Cauchy equation and the two linearly independent solutions are

$$\phi_1(\rho) = \rho^c, \quad \phi_2(\rho) = \rho^{-c}, \quad (3.36)$$

where $c = \sqrt{1 + \omega/\eta}$. Using equations (3.36), (3.24), and (3.10), the maximum hoop stress occurring at the inner surface can be found and is written as

$$(\sigma_\theta)_{\max} = \frac{P\xi}{\eta \tanh \xi}, \quad (3.37)$$

where $\xi \equiv c\eta = \sqrt{\eta^2 + \omega\eta}$. The maximum normalized hoop stress, $S = (\sigma_\theta)_{\max}/\sigma_0$, is given by

$$S = \frac{\xi \tanh \eta}{\eta \tanh \xi}. \quad (3.38)$$

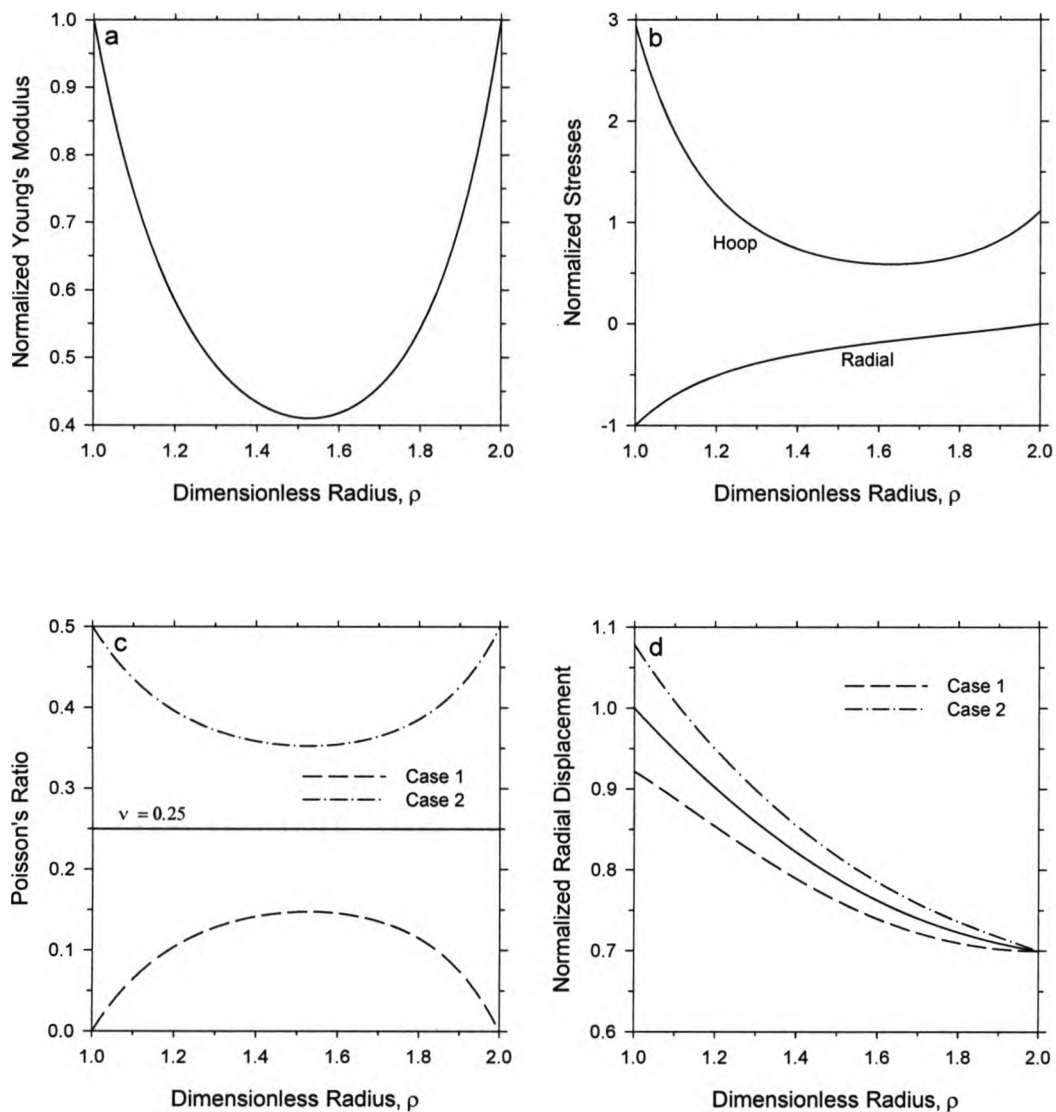


Figure 3.1: (a) Spatial variation of normalized Young's modulus E/E_α versus dimensionless radius ρ when the constants in equation (3.18) are set as $E_\alpha = E_\beta$, $m = -2$, $\gamma = 0.172$, and $s = 4.1$; (b) Distribution of normalized hoop and radial stresses, S_θ and S_ρ , versus dimensionless radius ρ ; (c) Different spatial variation of Poisson's ratio ν versus dimensionless radius ρ for $\nu_0 = 0.25$; (d) Distributions of corresponding normalized radial displacement u/u_0 versus dimensionless radius ρ .

For imaginary values of ξ , i.e. $\xi = i|\xi|$, the identity $\tanh(i|\xi|) = i \tan |\xi|$ is used. If $\omega = 0$ the material is homogeneous and $S = 1$. To show the effect of spatial variation of Poisson's ratio, a Taylor series expansion around $\omega = 0$ is found and the first two terms are given by

$$S \approx 1 + \left[1 - \frac{2\eta}{\sinh 2\eta} \right] \frac{\omega}{2\eta}. \quad (3.39)$$

The second term contains the effect of spatial variation of Poisson's ratio. The largest possible effect of the spatial variation occurs when $\omega = \pm 1/2$ and Fig. 3.2 shows the graph of S versus η for these cases. The Taylor series shows reasonable agreement with the exact result. For the values $\eta < 1/2$, the stress is approximately given by $S \approx 1 + \omega\eta/3$. As shown in the figure when $\eta \approx 1.3$, i.e. $\beta \approx 3.7$, there is at most a change of 12% in the hoop stress. For values of $\eta > 3$ the stress dies off according to $S \approx 1 + \omega/2\eta$.

3.5 Discussion and conclusions

The axisymmetric stress field in a pressurized ring where both Poisson's ratio and Young's modulus change continuously across the radius has been derived. Young's modulus is written as $E = E_a\zeta$ and here the function $\zeta = \rho^{2m} \exp[\gamma(\rho^s - 1)]$, which has been given in equation (3.18), is used. Using standard techniques in curve fitting, the parameters m , γ , and s can be adjusted to find the best fit for the actual stiffness profile. A rationale for writing Poisson's ratio in the form $\nu = \nu_0 + \nu_1\zeta$ has been presented in Section 3.2.3 where the parameters ν_0 and ν_1 are adjusted to fit the actual profile of Poisson's ratio.

The stress depends only upon E and ν_0 , whilst the displacement u also de-

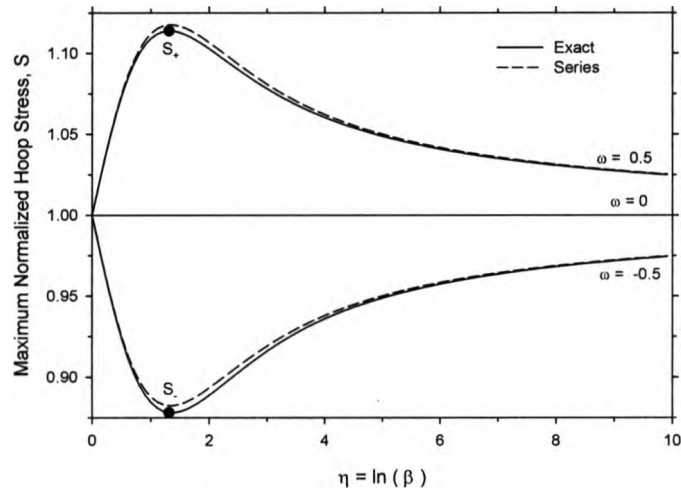


Figure 3.2: Distributions of exact and approximate maximum normalized hoop stress S versus $\eta = \ln \beta$ for $\omega = \pm 0.5$ and $\omega = 0$. When $\eta < 1/2$, the stress is approximately given by $S \approx 1 + \omega\eta/3$. The maximum and minimum stresses, $S_+ \approx 1.12$ and $S_- \approx 0.88$, differ by about 12% from the case where Poisson's ratio is constant, i.e. $\omega = 0$

depends on ν_1 . To investigate the effect of the nonconstant Poisson's ratio upon the elastic field, two situations have been considered. First, in Section 3.4.1, both the expression for the elastic modulus E and the numerical value of ν_0 are given. The stress is then completely defined and the effect of the parameter ν_1 upon the radial displacement is investigated. For the pressurized ring, the maximum value of u occurs at the inner surface and it has been found that by varying ν_1 between its limits, the radial displacement can change by up to 15%. Secondly, in Section 3.4.2, Young's modulus E is held constant and Poisson's ratio is allowed to vary across the wall thickness from ν_a to ν_b . The maximum change in ν across the wall thickness is then given when $\omega = \nu_b - \nu_a = \pm 1/2$. The maximum hoop stress occurs at the inner surface, and, depending upon the value of ω , this stress changes by up to $\pm 12\%$.

Bibliography

- [1] M. Sasaki and T. Hirai. Fabrication and properties of functionally graded materials. *Journal of the Ceramic Society of Japan*, 99:1002–1013, 1991.
- [2] Y. Miyamoto, W.A. Kaysser, R.H. Rabin, A. Kawasaki, and R.G. Ford. *Functionally Graded Materials: Design, Processing and Applications*. Kluwer Academic Publishers, USA, 1999.
- [3] V. Birman and L.W. Byrd. Modeling and analysis of functionally graded materials and structure. *Applied Mechanics Reviews*, 60:195–216, 2007.
- [4] A.J. Markworth, K.S. Ramesh, and W.P. Parks. Modelling studies applied to functionally graded materials. *Journal of Materials Science*, 30:2183–2193, 1995.
- [5] Y. Fukui, N. Yamanaka, and K. Wakashima. The stresses and strains in a thick-walled tube for functionally graded material under uniform thermal loading. *JSME International Journal A-Solid Mechanics*, 36:156–162, 1993.
- [6] M. Picasso, C.F. Marsden, J.D. Wagniere, A. Frenk, and M. Rappaz. A simple but realistic model for laser cladding. *Metallurgical and Materials Transactions B*, 25:281–291, 1994.
- [7] M.U. Islam. An overview of research in the fields of laser surface modification and laser machining at the integrated manufacturing technologies institute NRC. *Advanced Performance Materials*, 3:215–238, 1996.
- [8] M.S. Ozmusul and R.C. Picu. Elastic moduli of particulate compos-

- ites with graded filler-matrix interface. *Polymer Composites*, 23:110–119, 2002.
- [9] N. Noda. Thermal stresses in functionally graded materials. *Journal of Thermal Stresses*, 22:477–512, 1999.
- [10] M. Jabbari, S. Sohrabpour, and M.R. Eslami. Mechanical and thermal stresses in a functionally graded hollow cylinder due to radially symmetric loads. *International Journal of Pressure Vessels and Piping*, 79:493–497, 2002.
- [11] J.R. Dryden. Bending of inhomogeneous curved bars. *International Journal of Solids and Structures*, 44:4158–4166, 2007.
- [12] M. Mohammadi and J.R. Dryden. Thermal stresses in a nonhomogeneous curved beam. *Journal of Thermal Stresses*, 31:587–598, 2008.
- [13] P.R. Marur and H.V. Tippur. Evaluation of mechanical properties of functionally graded materials. *Journal of Testing and Evaluation*, 26:539–545, 1998.
- [14] M.P. Lutz and R.W. Zimmerman. Thermal stresses and effective thermal expansion coefficient of a functionally gradient sphere. *Journal of Thermal Stresses*, 19:39–54, 1996.
- [15] R.W. Zimmerman and M.P. Lutz. Thermal stresses and thermal expansion in a uniformly heated functionally graded cylinder. *Journal of Thermal Stresses*, 22:177–188, 1999.
- [16] G.H. Paulino and J-H. Kim. On the poisson's ratio effect on mixed-mode stress intensity factors and t-stress in functionally graded materials.

- International Journal of Computational Engineering Science, 5:833–861, 2004.
- [17] A.N. Eraslan. Stresses in FGM pressure tubes under non-uniform temperature distribution. *Structural Engineering and Mechanics*, 26:393–408, 2006.
- [18] A.E.H. Love. *A Treatise on the Mathematical Theory of Elasticity*. Cambridge University Press Warehouse, second edition, 1906.
- [19] S. Timoshenko and J.N. Goodier. *Theory of Elasticity*. McGraw-Hill, New York, third edition, 1970.
- [20] M. Braun. *Differential Equations and Their Applications*. Springer, New York, fourth edition, 1993.
- [21] J. Dryden and K. Jayaraman. Effect of inhomogeneity on the stress in pipes. *Journal Elasticity*, 83:179–189, 2006.
- [22] M. Abramowitz and I.A. Stegun, editors. *Handbook of Mathematical Functions*. Dover Publications, INC., New York, 1972.

Chapter 4

Stress Concentration around a Hole

4.1 Introduction

Functionally¹ graded materials (FGMs) were initially brought to scientific attention in 1984 [1]. These nonhomogeneous composites are used in various applications, see e.g. [2, 3]. The composition and morphology of FGMs gradually change over the volume; consequently, the elastic properties of the material change with position [4]. Of particular interest in this contribution is the special case where the elastic properties within an elastic body vary in the radial direction but are independent of tangential direction. This type of inhomogeneity can be due to several causes: directional cooling leading to a microstructural gradient [5]; phase segregation arising as a result of centrifugal casting [6]; and surface modification using laser technology [7].

¹M. Mohammadi, J. R. Dryden, L. Jiang, Stress Concentration around a Circular Hole in a Radially Nonhomogeneous Plate, Article In Press in International Journal of Solids and Structures, October 2010.

The elastic stress field in FGMs, where the elastic properties vary in the radial direction, has recently received considerable attention [8, 9, 10, 11]. For these types of FGMs most of the analytic investigation has been axisymmetric and directed toward pressurized FG tubes and disks [12, 13], curved beams [14, 15, 16], and thermal stress analysis [17, 18].

There has been less analytical investigation on the effect of radial inhomogeneity upon the elastic field in non-axisymmetric problems, see e.g. [19, 20]. Curved beams have been investigated by Lekhnitskii [21]. Other geometries such as hollow cylinders by Shao et al. [22], spheres by Poultangari et al. [23], pressurized vessels by Jabbari et al. [24], and spherical inclusions by Lutz and Zimmerman [25]. In most of these contributions power law functions have been used to define the variation of elastic properties. Here we want to calculate the stress field around a circular hole subjected to uniform far-field stress and power law functions are not suitable to define the spatial variation of Young's modulus in an infinite plate.

The stress concentration factor around a hole in a homogeneous plate has received much attention over the last decades see e.g. [26, 27]. In the case of functionally graded materials, some numerical work has been done recently. Using an isoparametric finite element formulation, Kubair and Bhanu-Chandar [28] investigated stress concentration around a circular hole in functionally graded panels under uniaxial tension. They found that the stress concentration factor was reduced when Young's modulus progressively decreases towards the hole. Subsequently, Yang et al. [29] investigated the stress field around a circular hole in a FGM plate. They used piece-wise homogeneous layers and complex variable methods. The plate was decomposed into N rings with equal thickness and constant material properties. The elastic fields for different spatial variations of the elastic properties were calculated.

The aim of this contribution is to present an analytical calculation for the stress concentration factor around a circular hole in an infinite plate made of an inhomogeneous material subjected to uniform biaxial tension and pure shear loading. Here, both Young's modulus and Poisson's ratio are smooth monotonic functions of the radius and attain limiting values far from the hole. Exponential functions are used to define the variation of elastic properties. A closed form expression for the stress concentration factor for biaxial tension is presented; the expression for the stress concentration factor for pure shear loading is obtained in terms of series solution. The influence of nonhomogeneous stiffness and varying Poisson's ratio on the stress concentration factor for both cases are then considered. Finally, an approximation for the stress concentration factor for pure shear loading is obtained.

4.2 Description of the Inhomogeneity

Consider an infinite plate with a circular hole of radius a where the plate is subjected to a uniform far-field stress. The presence of the hole changes the elastic field in the vicinity of the hole and to calculate the stress, polar coordinates are used. The radial coordinate, r , is normalized with respect to the radius of the hole, and a dimensionless radius is then defined as $\rho = r/a$. The elastic solid is nonhomogeneous and it is considered to be isotropic. The material properties change in the radial direction and approach uniform values at distances far away from the hole. As described in Section 4.1, this type of nonhomogeneity can be due to several reasons. With this behavior in mind, a dimensionless function $\kappa(\rho)$ is introduced and Young's modulus E is written

as

$$E = E_{\infty} \kappa(\rho). \quad (4.1)$$

Similarly, Poisson's ratio is expressed as

$$\nu = \nu_0 + (\nu_{\infty} - \nu_0) \kappa(\rho). \quad (4.2)$$

There are many functions that can be used to describe the behavior of κ and here the only restrictions are that

$$\kappa(\infty) = 1, \quad \kappa_1 \equiv \frac{E_1}{E_{\infty}} \equiv \kappa(1) > 0, \quad (4.3)$$

where E_1 and ν_1 are the properties at $\rho = 1$. At large distances from the hole $E = E_{\infty}$ and $\nu = \nu_{\infty}$; whereas at the periphery of the hole, $E_1 = E_{\infty} \kappa_1$ and $\nu_1 = \nu_0 + (\nu_{\infty} - \nu_0) \kappa_1$. The parameter ν_0 is adjustable.

4.3 Governing Differential Equation

Suppose that the plate is subjected to a uniform far-field stress. Near the hole the uniform elastic field is perturbed and a polar coordinate system is used to calculate the stresses. The basic elastic equations for plane stress are given [30]. First, the displacement components U and V , in the radial and tangential directions respectively, are normalized, $u = U/a$ and $v = V/a$. The strain-displacement relations are well known see for example [30] and the relevant terms are

$$\epsilon_{\rho} = \frac{\partial u}{\partial \rho}, \quad (4.4)$$

$$\epsilon_{\theta} = \frac{u}{\rho} + \frac{1}{\rho} \frac{\partial v}{\partial \theta}, \quad (4.5)$$

$$\gamma_{\rho\theta} = \frac{\partial v}{\partial \rho} - \frac{v}{\rho} + \frac{1}{\rho} \frac{\partial u}{\partial \theta}, \quad (4.6)$$

where ϵ_{ρ} , ϵ_{θ} , and $\gamma_{\rho\theta}$ represent the normal and shear strain components respectively. The compatibility equation is given in reference [31] and is written as

$$\frac{\partial}{\partial \rho} \left(\frac{\partial(\rho\epsilon_{\theta})}{\partial \rho} - \epsilon_{\rho} \right) + \frac{1}{\rho} \frac{\partial^2 \epsilon_{\rho}}{\partial \theta^2} = \frac{1}{\rho} \frac{\partial}{\partial \theta} \left(\frac{\partial \gamma_{\rho\theta}}{\partial \rho} + \frac{\gamma_{\rho\theta}}{\rho} \right). \quad (4.7)$$

The normal and shear stresses are labeled as σ_{ρ} , σ_{θ} , and $\tau_{\rho\theta}$ respectively. The two equilibrium equations are given by [30]:

$$\rho - \text{direction} : \frac{\partial \sigma_{\rho}}{\partial \rho} + \frac{1}{\rho} \frac{\partial \tau_{\rho\theta}}{\partial \theta} + \frac{\sigma_{\rho} - \sigma_{\theta}}{\rho} = 0, \quad (4.8)$$

$$\theta - \text{direction} : \frac{1}{\rho} \frac{\partial \sigma_{\theta}}{\partial \theta} + \frac{\partial \tau_{\rho\theta}}{\partial \rho} + \frac{2\tau_{\rho\theta}}{\rho} = 0. \quad (4.9)$$

The solid is a linear elastic material and in plane stress; Hooke's law is written as

$$\epsilon_{\rho} = \frac{1}{E} (\sigma_{\rho} - \nu \sigma_{\theta}), \quad (4.10)$$

$$\epsilon_{\theta} = \frac{1}{E} (\sigma_{\theta} - \nu \sigma_{\rho}), \quad (4.11)$$

$$\gamma_{\rho\theta} = \frac{2(1+\nu)}{E} \tau_{\rho\theta}, \quad (4.12)$$

where E and ν are defined by equations (4.1) and (4.2) respectively. It is noted that, the average values of displacement, strain, and stress across the thickness are used in this study and for the sake of simplicity the overbar is omitted from all of these average values [32].

If $\psi(\rho, \theta)$ is the stress function, then the stress components are given by

$$\sigma_\rho = \frac{1}{\rho} \frac{\partial \psi}{\partial \rho} + \frac{1}{\rho^2} \frac{\partial^2 \psi}{\partial \theta^2}, \quad (4.13)$$

$$\sigma_\theta = \frac{\partial^2 \psi}{\partial \rho^2}, \quad (4.14)$$

$$\tau_{\rho\theta} = \frac{1}{\rho^2} \frac{\partial \psi}{\partial \theta} - \frac{1}{\rho} \frac{\partial^2 \psi}{\partial \rho \partial \theta}. \quad (4.15)$$

It is well known that the stress components defined in this way satisfy the equilibrium equations [31]. Combining the above equations, the strain can be written in terms of the stress function:

$$E_\infty \epsilon_\rho = \frac{1}{\kappa} \left(\frac{1}{\rho} \frac{\partial \psi}{\partial \rho} + \frac{1}{\rho^2} \frac{\partial^2 \psi}{\partial \theta^2} - \nu_0 \frac{\partial^2 \psi}{\partial \rho^2} \right) - (\nu_\infty - \nu_0) \left(\frac{\partial^2 \psi}{\partial \rho^2} \right), \quad (4.16)$$

$$E_\infty \epsilon_\theta = \frac{1}{\kappa} \left(\frac{\partial^2 \psi}{\partial \rho^2} - \frac{\nu_0}{\rho} \frac{\partial \psi}{\partial \rho} - \frac{\nu_0}{\rho^2} \frac{\partial^2 \psi}{\partial \theta^2} \right) - (\nu_\infty - \nu_0) \left(\frac{1}{\rho} \frac{\partial \psi}{\partial \rho} + \frac{1}{\rho^2} \frac{\partial^2 \psi}{\partial \theta^2} \right), \quad (4.17)$$

$$E_\infty \gamma_{\rho\theta} = \frac{2(1 + \nu_0)}{\kappa} \left(\frac{1}{\rho^2} \frac{\partial \psi}{\partial \theta} - \frac{1}{\rho} \frac{\partial^2 \psi}{\partial \rho \partial \theta} \right) + 2(\nu_\infty - \nu_0) \left(\frac{1}{\rho^2} \frac{\partial \psi}{\partial \theta} - \frac{1}{\rho} \frac{\partial^2 \psi}{\partial \rho \partial \theta} \right) \quad (4.18)$$

where κ , ν_0 , and ν_∞ are defined in equation (4.1) and (4.2). By inserting

equations (4.16-4.18) into the compatibility condition (4.7), the governing partial differential equation for the stress function $\psi(\rho, \theta)$ is obtained and written as:

$$\begin{aligned} \nabla^2 \nabla^2 \psi - \frac{\kappa'}{\kappa} \left\{ 2 \frac{\partial^3 \psi}{\partial \rho^3} + \left(\frac{2 - \nu_0}{\rho} \right) \frac{\partial^2 \psi}{\partial \rho^2} - \frac{1}{\rho^2} \frac{\partial \psi}{\partial \rho} - \frac{3}{\rho^3} \frac{\partial^2 \psi}{\partial \theta^2} + \frac{2}{\rho^2} \frac{\partial^3 \psi}{\partial \theta^2 \partial \rho} \right\} \\ + \frac{2\kappa'^2 - \kappa''\kappa}{\kappa^2} \left\{ \frac{\partial^2 \psi}{\partial \rho^2} - \frac{\nu_0}{\rho} \frac{\partial \psi}{\partial \rho} - \frac{\nu_0}{\rho^2} \frac{\partial^2 \psi}{\partial \theta^2} \right\} = 0, \end{aligned} \quad (4.19)$$

where ' and '' are the first and second total derivatives with respect to ρ . The biharmonic equation $\nabla^2 \nabla^2 \psi$ is defined by

$$\nabla^2 \nabla^2 \psi = \left(\frac{\partial^2}{\partial \rho^2} + \frac{1}{\rho} \frac{\partial}{\partial \rho} + \frac{1}{\rho^2} \frac{\partial^2}{\partial \theta^2} \right) \left(\frac{\partial^2 \psi}{\partial \rho^2} + \frac{1}{\rho} \frac{\partial \psi}{\partial \rho} + \frac{1}{\rho^2} \frac{\partial^2 \psi}{\partial \theta^2} \right). \quad (4.20)$$

For the case of homogeneous materials, κ is constant and equation (4.19) reduces to $\nabla^2 \nabla^2 \psi = 0$, see for example [30, 32]. It is noted that the terms involving $\nu_\infty - \nu_0$ do not enter into the final governing differential equation (4.19) and the stress function only depends on ν_0 .

4.3.1 The general form of the stress function

The stress function ψ is assigned the separable form

$$\psi(\rho, \theta) = f(\rho) \cos(m\theta), \quad (4.21)$$

and upon substituting this into equation (4.19), the governing equation reduces to an ordinary differential equation which is

$$\rho^4 f'''' + \rho^3 [2 - 2g] f''' + \rho^2 [g(\nu_0 - 2) + h - 1 - 2m^2] f''$$

$$+\rho \left[(g+1)(1+2m^2) - h\nu_0 \right] f' + \left[m^4 + m^2(h\nu_0 - 3g - 4) \right] f = 0, \quad (4.22)$$

where g and h are dimensionless functions that describe the nonhomogeneity:

$$g = \frac{\rho\kappa'}{\kappa}, \quad (4.23)$$

$$h = g^2 + g - g'\rho. \quad (4.24)$$

Here we want to calculate the stress concentration factor around a hole subjected to: 1) biaxial loading, $m = 0$, as shown in Fig. 1(a), and 2) pure shear, $m = 2$, as shown in Fig. 1(b). The former is an axisymmetric problem, while the latter is non-axisymmetric.

4.4 Stress State due to biaxial Tension: $m = 0$

Consider the far-field stress corresponding to $m = 0$ as shown in Fig. 4.1(a). The governing differential equation (4.22) becomes

$$\begin{aligned} \rho^4 f'''' + 2\rho^3 [1 - g] f''' \\ + \rho^2 [g(\nu_0 - 2) + h - 1] f'' + \rho [g + 1 - h\nu_0] f' = 0, \end{aligned} \quad (4.25)$$

and this represents an axisymmetric stress field. After some algebra, it can be verified that equation (4.25) can be written as

$$\left[\frac{\rho}{\kappa} \left\{ f''' + \left(\frac{1-g}{\rho} \right) f'' - \left(\frac{1-\nu_0 g}{\rho^2} \right) f' \right\} \right]' = 0. \quad (4.26)$$

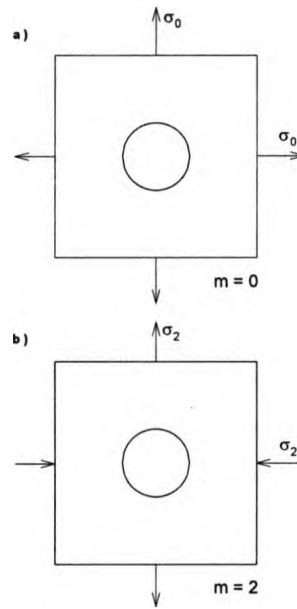


Figure 4.1: Far-field loading on the plate containing the circular hole: a) shows the biaxial loading σ_0 , corresponding to $m = 0$; and b) shows pure shear σ_2 , corresponding to $m = 2$

Defining $p \equiv f'$, the governing differential equation is then reduced to

$$p'' + \left(\frac{1-g}{\rho}\right) p' - \left(\frac{1-\nu_0 g}{\rho^2}\right) p = \frac{\varepsilon \kappa}{\rho}, \quad (4.27)$$

where the coefficient ε is the constant of integration. The particular solution of equation (4.27) associated with the constant ε corresponds to the bending problem and is not required here.

The periphery of the hole is stress free and the radial stress is equal to σ_0 at infinity; therefore, the boundary conditions for this problem are

$$p(1) = 0, \quad \lim_{\rho \rightarrow \infty} \frac{p}{\rho} = \sigma_0. \quad (4.28)$$

Suppose that p_1 and p_2 are two linearly independent solutions of equation

(4.27) where the constant ε is set equal to zero. Considering the boundary conditions (4.28), the stress function p is written as

$$p = \sigma_0 \left(\frac{p_1(\rho) p_2(1) - p_2(\rho) p_1(1)}{p_2(1)} \right). \quad (4.29)$$

The stress concentration factor, K_0 , corresponding to hydrostatic loading can be found from this stress function.

The factor K_0 is defined as the ratio of the maximum hoop stress which occurs at $\rho = 1$ to the reference stress σ_0 [27]. Using equations (4.14) and (4.29), it follows that

$$K_0 = \frac{p_1'(1) p_2(1) - p_2'(1) p_1(1)}{p_2(1)}. \quad (4.30)$$

The numerator of equation (4.30) is equal to the Wronskian evaluated at $\rho = 1$, see for example [33]. In this case the Wronskian, $W = p_1' p_2 - p_2' p_1 = C\kappa(\rho)/\rho$ where $\kappa(\rho)$ is defined in equation (4.1). The elastic properties become uniform at large distances away from the hole, i.e. $\kappa(\infty) = 1$, so that the solutions must be such that $p_1 \sim \rho$ and $p_2 \sim 1/\rho$. It then follows that the constant $C = 2$ and the Wronskian can be written as $W = 2\kappa(\rho)/\rho$. The stress concentration factor is then expressed as

$$K_0 = 2 \left(\frac{E_1}{E_\infty} \right) \Sigma_0, \quad (4.31)$$

where the normalized stress concentration factor Σ_0 is

$$\Sigma_0 = \frac{1}{p_2(1)}. \quad (4.32)$$

It is noted that, Σ_0 is a function of s , ν_0 , and E_1/E_∞ . To obtain an analytical

expression for K_0 , a definite form must be assigned to the function $\kappa(\rho)$.

4.4.1 Spatial variation of $\kappa(\rho)$

For the kind of inhomogeneity envisaged in this paper there are two main features. First, there is the value of the stiffness at the hole periphery, and secondly, there is the rate at which the inhomogeneity decays away from the hole. These two features can be captured by the following expression:

$$\kappa(\rho) = \exp(x), \quad \text{where} \quad x = \eta\rho^s, \quad (4.33)$$

where η and $s < 0$ are adjustable parameters. The parameter η determines the stiffness at the hole perimeter and s determines the decay rate away from the hole. The function $\kappa(\rho)$ monotonically approaches unity as ρ increases.

For the spatial variation $E = E_\infty \exp[\eta\rho^s]$, the solutions p_1 and p_2 are known [13]. They are given by

$$p_1 = \rho M\left(\frac{1-\nu_0}{s}, 1 + \frac{2}{s}, \eta\rho^s\right), \quad p_2 = \frac{1}{\rho} M\left(-\frac{1+\nu_0}{s}, 1 - \frac{2}{s}, \eta\rho^s\right), \quad (4.34)$$

where $M(a, b, x)$ is the Kummer's function and some of the basic properties of Kummer's function can be found in references [34, 35]. Using equations (4.31), (4.33), and (4.34), K_0 is written as

$$K_0 = 2 \exp(\eta) \Sigma_0, \quad (4.35)$$

where considering equation (4.33) the coefficient

$$\exp(\eta) = \frac{E_1}{E_\infty}, \quad (4.36)$$

and the normalized stress concentration factor Σ_0 is given by

$$\Sigma_0 = \frac{1}{M\left(-\frac{1+\nu_0}{s}, 1 - \frac{2}{s}, \eta\right)}. \quad (4.37)$$

If this expression for Σ_0 is expanded as a power series in η it becomes clear that there are two limiting cases corresponding to small and large values for $|s|$

$$\Sigma_0 \sim \begin{cases} 1 & |s| \gg 1, \\ \exp[-(1 + \nu_0)\eta/2] & |s| \ll 1. \end{cases} \quad (4.38)$$

For the case of homogeneous materials, $\eta = 0$, and the stress concentration factor reduces to the well-known result, [27], $K_0 = 2$.

4.5 Stress State due to Pure Shear Loading:

$$m = 2$$

Far field stresses $\sigma_y = \sigma_2$ and $\sigma_x = -\sigma_2$ are applied as shown in Fig. 1(b). The periphery of the hole is stress free. The stress function is then written as

$$\psi(\rho, \theta) = f(\rho) \cos(2\theta). \quad (4.39)$$

The problem is non-axisymmetric and the shear stress is not zero in this case. Assuming the functional form for $\kappa(\rho)$ proposed in equation (4.33), the governing differential equation (4.22) becomes

$$\begin{aligned} \rho^4 f'''' + 2[1 - sx] \rho^3 f'''' - [9 - (\nu_0 - 1 - s)sx - s^2 x^2] \rho^2 f'' \\ + [9 + (9 + \nu_0 s - \nu_0)sx - \nu_0 s^2 x^2] \rho f' \end{aligned} \quad (4.40)$$

$$+ \left[4(\nu_0 - \nu_0 s - 3)sx + 4\nu_0 s^2 x^2 \right] f = 0.$$

The periphery of the hole is stress free so that, the boundary conditions are written as

$$\sigma_\rho(1) = 0, \quad \tau_{\rho\theta}(1) = 0, \quad \lim_{\rho \rightarrow \infty} \sigma_\rho \Big|_{\theta=0} = -\sigma_2. \quad (4.41)$$

Using equations (4.13), (4.15), and (4.39), the boundary conditions in terms of $f(\rho)$ are

$$\lim_{\rho \rightarrow \infty} \left(\frac{f'(\rho)}{\rho} - \frac{4f(\rho)}{\rho^2} \right) = -\sigma_2, \quad (4.42)$$

$$f'(1) = 0, \quad (4.43)$$

$$f(1) = 0. \quad (4.44)$$

The independent solutions of governing equation (4.40) must be found and adjusted to fit the boundary conditions (4.42-4.44). After finding these solutions and applying the boundary conditions, the state of stress and consequently, the stress concentration factor can be determined.

4.5.1 Series Solution

A closed form solution is not possible and here a series solution is used. The function $f(\rho)$ is written as a power series

$$f(\rho) = \rho^q \sum_{n=0}^{\infty} \mathcal{A}_n x^n, \quad (4.45)$$

where q is an unknown constant. Substituting equation (4.45) into the governing differential equation (4.40) leads to the recursion formula

$$\rho^q \sum_{n=0}^{\infty} \{\alpha_n \mathcal{A}_n + \beta_{n-1} \mathcal{A}_{n-1} + \gamma_{n-2} \mathcal{A}_{n-2}\} x^n = 0, \quad (4.46)$$

where the coefficients $\mathcal{A}_{-1} = \mathcal{A}_{-2} \equiv 0$. The terms α_n , β_n , and γ_n are found as

$$\begin{aligned} \alpha_n &= (q + ns - 4)(q + ns - 2)(q + ns)(q + ns + 2), \\ \beta_n &= s(q + ns) [(q + ns - 1) \{-2(q + ns) + \nu_0 + 3 - s\} + 9 + \nu_0 s - \nu_0] \\ &\quad + 4s(\nu_0 - \nu_0 s - 3), \\ \gamma_n &= s^2(q + ns) [q + ns - 1 - \nu_0] + 4s^2 \nu_0. \end{aligned} \quad (4.47)$$

Setting $n = 0$ in equation (4.46) yields $\alpha_0 \mathcal{A}_0 = 0$ and since $\mathcal{A}_0 \neq 0$ it follows that the indicial equation for q corresponds to

$$\alpha_0 = q(q - 4)(q - 2)(q + 2) = 0. \quad (4.48)$$

The indicial roots are then $q = (2, -2, 0, 4)$. An independent solution is associated with each root q of the indicial equation. For values of $n > 0$ the coefficients \mathcal{A}_n are deduced by the recursive relations

$$\begin{aligned} \alpha_1 \mathcal{A}_1 + \beta_0 \mathcal{A}_0 &= 0, & n = 1, \\ \alpha_2 \mathcal{A}_2 + \beta_1 \mathcal{A}_1 + \gamma_0 \mathcal{A}_0 &= 0, & n = 2, \\ \alpha_3 \mathcal{A}_3 + \beta_2 \mathcal{A}_2 + \gamma_1 \mathcal{A}_1 &= 0, & n = 3, \\ &\vdots & \vdots \\ \alpha_n \mathcal{A}_n + \beta_{n-1} \mathcal{A}_{n-1} + \gamma_{n-2} \mathcal{A}_{n-2} &= 0, \end{aligned} \quad (4.49)$$

where \mathcal{A}_0 is an arbitrary constant and the coefficients $\mathcal{A}_1, \mathcal{A}_2, \dots$ can be found as multiples of \mathcal{A}_0 . The solution corresponding to $q = 4$ gives unbounded stress as $\rho \rightarrow \infty$ and is not used here.

Now, the solutions corresponding to $q = (2, -2, 0)$ are calculated and the procedure is discussed. It is noted that, f_1 corresponds to $q = 2$; f_2 corresponds to $q = -2$; and f_3 corresponds to $q = 0$. Here, using the recursive formula (4.46) and (4.49), the three solutions of the governing differential equation (4.40) when $m = 2$ are determined.

4.5.2 Solution corresponding to uniform far-field stress

Consider $f_1(\rho)$ as the first general solution corresponding to $q = 2$. This solution refers to uniform far-field stress and using equation (4.45), it is written as

$$f_1(\rho) = \frac{\rho^2}{2} \sum_{n=0}^{\infty} F_n x^n, \quad (4.50)$$

where the coefficients F_n are defined from

$$\begin{aligned} \alpha_1 F_1 + \beta_0 F_0 &= 0, & n = 1, \\ \alpha_2 F_2 + \beta_1 F_1 + \gamma_0 F_0 &= 0, & n = 2, \\ \alpha_3 F_3 + \beta_2 F_2 + \gamma_1 F_1 &= 0, & n = 3, \\ &\vdots & \vdots \\ \alpha_n F_n + \beta_{n-1} F_{n-1} + \gamma_{n-2} F_{n-2} &= 0, \end{aligned} \quad (4.51)$$

where the coefficients α_n , β_n , and γ_n are

$$\begin{aligned} \alpha_n &= ns(ns + 4)(ns - 2)(ns + 2), \\ \beta_n &= s(2 + ns) [(1 + ns) \{-2ns + \nu_0 - 1 - s\} + 9 + \nu_0 s - \nu_0] \end{aligned}$$

$$\begin{aligned}
 &+ 4s(\nu_0 - \nu_0s - 3), \\
 \gamma_n &= s^2(2 + ns)[ns + 1 - \nu_0] + 4s^2\nu_0.
 \end{aligned} \tag{4.52}$$

The coefficients

$$\begin{aligned}
 F_1 &= \left[\frac{2(1 + \nu_0)}{(s + 4)(s + 2)} \right] F_0, \\
 F_2 &= \left[\frac{(1 + \nu_0)(2s^2 + s^3 - 2 - \nu_0s^2 - 2\nu_0 - 4s)}{4(s + 4)(s + 2)^2(s + 1)(s - 1)} \right] F_0,
 \end{aligned} \tag{4.53}$$

are the first two terms of the series (4.50) and F_0 is an arbitrary constant. For the sake of brevity, the other coefficients are not given. In addition the coefficient F_0 is arbitrary and is considered as $F_0 = 1$.

4.5.3 Solution associated with $q = -2$

The solution $f_2(\rho)$ corresponds to the root $q = -2$ and is written as

$$f_2(\rho) = \frac{1}{2\rho^2} \sum_{n=0}^{\infty} G_n x^n, \tag{4.54}$$

where the coefficients G_n are defined from

$$\begin{aligned}
 \alpha_1 G_1 + \beta_0 G_0 &= 0, & n = 1, \\
 \alpha_2 G_2 + \beta_1 G_1 + \gamma_0 G_0 &= 0, & n = 2, \\
 \alpha_3 G_3 + \beta_2 G_2 + \gamma_1 G_1 &= 0, & n = 3, \\
 \vdots & \quad \quad \quad \vdots & \\
 \alpha_n G_n + \beta_{n-1} G_{n-1} + \gamma_{n-2} G_{n-2} &= 0,
 \end{aligned} \tag{4.55}$$

$$\alpha_n H_n + \beta_{n-1} H_{n-1} + \gamma_{n-2} H_{n-2} = 0,$$

where the coefficients α_n , β_n , and γ_n are

$$\begin{aligned}\alpha_n &= ns(ns-4)(ns-2)(ns+2), \\ \beta_n &= ns^2 [(ns-1) \{-2ns + \nu_0 + 3 - s\} + 9 + \nu_0 s - \nu_0] \\ &\quad + 4s(\nu_0 - \nu_0 s - 3), \\ \gamma_n &= ns^3 [ns - 1 - \nu_0] + 4s^2 \nu_0.\end{aligned}\tag{4.60}$$

The first two coefficients are then written as

$$\begin{aligned}H_1 &= \left[\frac{4(\nu_0 s + 3 - \nu_0)}{(s-4)(s-2)(s+2)} \right] H_0, \\ H_2 &= \left[\frac{2s^3 \nu_0 - \nu_0 s^2 - 2\nu_0^2 s^2 + 9s^2 - 4\nu_0 s + 4\nu_0^2 s - 2\nu_0^2 + 12\nu_0 - 18}{4(s-4)(s-2)(s-1)(s+1)(s+2)} \right] H_0.\end{aligned}\tag{4.61}$$

Like previous solutions, the coefficient $H_0 = 1$.

4.5.5 The stress function $f(\rho)$ and stress concentration factor K_2

Considering the boundary conditions (4.42-4.44) and using the three solutions defined in (4.50), (4.54), and (4.58), the stress function can be determined and it is written as

$$f(\rho) = \sigma_2 \left(\frac{[f_2 f_3' - f_3 f_2']_1 f_1(\rho) + [f_3 f_1' - f_1 f_3']_1 f_2(\rho) + [f_1 f_2' - f_2 f_1']_1 f_3(\rho)}{[f_2 f_3' - f_3 f_2']_1} \right)\tag{4.62}$$

where the terms $[\dots]_1$ indicate evaluation at $\rho = 1$. Far from the hole, when $\rho \gg 1$, the stress function $f \sim \sigma_2 \rho^2/2$ corresponding to uniform far-field stress. Here, the stress function $f(\rho)$ is approximated by a truncated series containing terms up to η^N .

The hoop stress is given by $\sigma_\theta = f''(\rho) \cos(2\theta)$ and attains its maximum value at $\theta = 0$ on the periphery of the hole; thus, the stress concentration factor for the pure shear case, i.e. $m = 2$, is written as

$$K_2 = \left[\frac{(f_2 f'_3 - f_3 f'_2) f''_1 + (f_3 f'_1 - f_1 f'_3) f''_2 - (f_2 f'_1 - f_1 f'_2) f''_3}{f_2 f'_3 - f_3 f'_2} \right]_1. \quad (4.63)$$

In the same vein as equation (4.35), K_2 is written as

$$K_2 = 4 \left(\frac{E_1}{E_\infty} \right) \Sigma_2, \quad (4.64)$$

where the normalized stress concentration factor Σ_2 is given by

$$\Sigma_2 = 1 + a_1 \eta + \frac{a_2 \eta^2}{2!} + \frac{a_3 \eta^3}{3!} + \dots + \frac{a_N \eta^N}{N!}, \quad (4.65)$$

where the coefficients a_1, \dots are known and they are functions of ν_0 and s . Upon inspection of the series terms, two limiting cases, corresponding to small and large values for $|s|$, are observed to be given by

$$\Sigma_2 \sim \begin{cases} 1 & |s| \gg 1, \\ \exp[(\nu_0 - 3)\eta/4] & |s| \ll 1. \end{cases} \quad (4.66)$$

For the case of homogeneous materials, $\eta = 0$, and the stress concentration factor reduces to the well-known result, [27], $K_2 = 4$.

4.6 Results and Discussion

Suppose that the plate is subjected to uniform far-field stress with components σ_x and σ_y . By inspection of Figs. (4.1 a) and (4.1 b), it is clear that $\sigma_x = \sigma_0 - \sigma_2$ and $\sigma_y = \sigma_0 + \sigma_2$. It then follows that

$$\sigma_0 = \frac{\sigma_y + \sigma_x}{2}, \quad \text{and} \quad \sigma_2 = \frac{\sigma_y - \sigma_x}{2}. \quad (4.67)$$

For uniaxial tension, $\sigma_x = 0$, and using superposition, the stress concentration factor is

$$K = \left(\frac{E_1}{E_\infty} \right) (\Sigma_0 + 2\Sigma_2). \quad (4.68)$$

When $\eta = 0$ this reduces to the well-known result $K = 3$.

Here, the elastic stiffness is given by $E = E_\infty \exp(\eta\rho^s)$ where $s < 0$. The far-field stiffness, $E = E_\infty$, is attained when $\rho^s \approx 0$. The requirement for ρ^s to become arbitrarily small can be written as $(1 + t)^s = e^m$ where $m < 0$. Upon solving for t , it is found that

$$t = e^{\frac{m}{s}} - 1 = \frac{m}{s} + \frac{1}{2} \left(\frac{m}{s} \right)^2 + \frac{1}{3!} \left(\frac{m}{s} \right)^3 + \dots \quad (4.69)$$

The convergence of this estimate for t depends on the ratio m/s . For simplicity $m = -1$ and t is estimated as

$$t = -\frac{1}{s}. \quad (4.70)$$

This gives a characteristic parameter to estimate the width of the inhomogeneous zone surrounding the hole and it is similar to the use of a characteristic time in electrical engineering. Fig. 4.2 shows the distribution of $\ln E/E_\infty$ versus the dimensionless radius ρ for different values of η and t . This section is divided into two parts. First, Poisson's ratio is considered as constant and

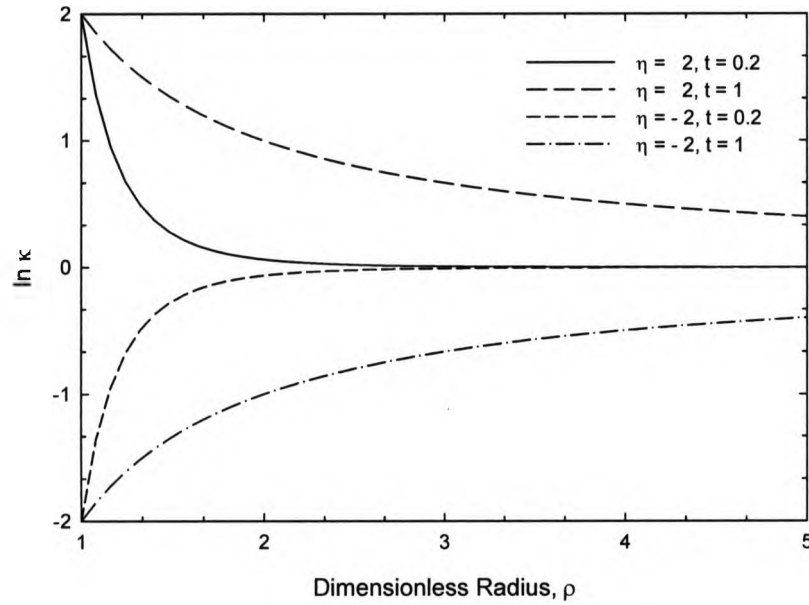


Figure 4.2: Graph of normalized Young's modulus $\ln \kappa(\rho)$, defined in equation (4.33), versus dimensionless radius ρ for the values of η and t shown

the effect of nonhomogeneous stiffness on the stress concentration factors is discussed. Secondly, Young's modulus is held constant and the influence of varying Poisson's ratio is analyzed.

4.6.1 Effect of nonhomogeneous stiffness upon K_0

For biaxial loading the stress concentration factor is $K_0 = 2(E_1/E_\infty)\Sigma_0$ where the function Σ_0 is given in equation (4.37) and using equation (4.70) for t

$$\Sigma_0 = \frac{1}{M(t + t\nu_0, 1 + 2t, \eta)}, \quad (4.71)$$

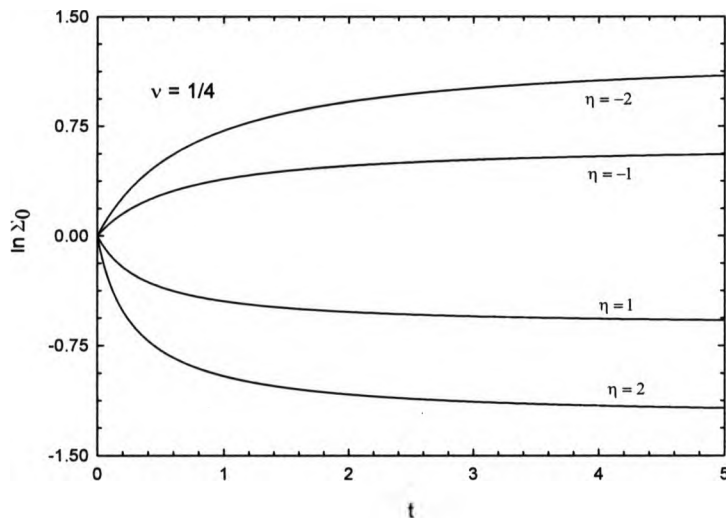


Figure 4.3: Graph of $\ln \Sigma_0$ versus t for the values of η shown and Poisson's ratio $\nu_0 = 1/4$. At $t = 0$ the slope is given by equation (4.72). For large values of t the limiting values $\pm 5\eta/8$ are attained

where $M(a, b, x)$ is the Kummer's function. When $t = 0$ the function $\Sigma_0 = 1$ and its derivative is given by

$$\left. \frac{\partial \Sigma_0}{\partial t} \right|_0 = -(1 + \nu_0) \left(\eta + \frac{\eta^2}{2 \times 2!} + \frac{\eta^3}{3 \times 3!} + \frac{\eta^4}{4 \times 4!} + \dots \right). \quad (4.72)$$

When $t \gg 1$ the function Σ_0 approaches the limit $L_0 = \exp[-(1 + \nu_0)\eta/2]$ as given in equation (4.38). Fig. 4.3 shows a graph of $\ln \Sigma_0$ versus t for various values of η and Poisson's ratio $\nu = \nu_0 = 1/4$. As t becomes large, $\ln \Sigma_0 \sim \pm 5\eta/8$. The most rapid change in Σ_0 occurs in the region $0 < t < 1$ and a Taylor's expansion around $t = 0$ requires too many terms to be very useful. However, commonly available software packages such as MAPLE allow convenient evaluation of the Kummer's function. The behavior of K_0 for other values of ν_0 is similar.

4.6.2 Effect of nonhomogeneous stiffness upon K_2

For the case of pure shear, the stress concentration factor is $K_2 = 4(E_1/E_\infty)\Sigma_2$ where the function Σ_2 is given in equation (4.65)

$$\Sigma_2 = 1 + a_1\eta + \frac{a_2\eta^2}{2!} + \frac{a_3\eta^3}{3!} + \frac{a_4\eta^4}{4!} + \frac{a_5\eta^5}{5!}.$$

The number of terms required for the series to converge evidently depends upon the magnitude of η and as might be expected, the terms get more complicated as N becomes large. Moving into the plate, from the far field to the periphery of the hole, the stiffness changes by a factor $\exp(\eta)$. In most FGMs this change is not exceedingly large and the value of η is likely less than 2. For this value of η the series gives a reasonable estimate if it is truncated when $N = 5$. The coefficients a_1, a_2, \dots, a_5 depend on $t = -1/s$ and ν_0 . The coefficient $a_1 = (b_{10} + b_{11}\nu_0)/c_1$ and is written as

$$a_1 = \frac{-3t - 12t^2 - 36t^3}{1 + 12t + 44t^2 + 48t^3} + \frac{\nu_0(-t + 8t^2 + 12t^3)}{1 + 12t + 44t^2 + 48t^3}. \quad (4.73)$$

The second coefficient has the form $a_2 = (b_{20} + b_{21}\nu_0 + b_{22}\nu_0^2)/c_2$ and is written as

$$\begin{aligned} \frac{b_{20}}{c_2} &= \frac{-3t - 27t^2 - 81t^3 + 180t^4 + 1938t^5 + 7128t^6 + 13608t^7 + 7776t^8}{2 + 56t + 662t^2 + 4304t^3 + 16784t^4 + 40064t^5 + 56928t^6 + 43776t^7 + 13824t^8}, \\ \frac{b_{21}}{c_2} &= \frac{-t + 14t^2 + 115t^3 + 112t^4 - 2544t^5 - 11088t^6 - 14256t^7 - 5184t^8}{2 + 56t + 662t^2 + 4304t^3 + 16784t^4 + 40064t^5 + 56928t^6 + 43776t^7 + 13824t^8}, \\ \frac{b_{22}}{c_2} &= \frac{3t^2 - 28t^3 - 68t^4 + 542t^5 + 1848t^6 + 2088t^7 + 864t^8}{2 + 56t + 662t^2 + 4304t^3 + 16784t^4 + 40064t^5 + 56928t^6 + 43776t^7 + 13824t^8}. \end{aligned}$$

Subsequent coefficients have the form $a_n = (b_{n0} + b_{n1}\nu_0 + \dots + b_{nn}\nu_0^n)/C_n$ but become too unwieldy to be useful and they are not presented.

When $t = 0$ the function $\Sigma_2 = 1$ and its derivative is given by

$$\vartheta \equiv \left. \frac{\partial \Sigma_2}{\partial t} \right|_0 = -(3 + \nu_0) \left(\eta + \frac{\eta^2}{2 \times 2!} + \frac{\eta^3}{3 \times 3!} + \frac{\eta^4}{4 \times 4!} + \dots \right). \quad (4.74)$$

When $t \gg 1$ the function Σ_2 approaches the limit $L_2 = \exp[(\nu_0 - 3)\eta/4]$ as given in equation (4.66). Fig. 4.4 shows a graph of $\ln \Sigma_2$ versus t for various values of η and Poisson's ratio $\nu = \nu_0 = 1/4$. The solid lines in Fig. 4.4 represent the series solution and the dashed lines are found from an approximate method which is described later. The most rapid change in Σ_2 occurs in the region $0 < t < 1$ and a Taylor's expansion around $t = 0$ requires too many terms to be very useful. As t becomes large, $\ln \Sigma_2 \sim \pm 11 \eta/16$. The behavior of Σ_2 is qualitatively similar to that of Σ_0 . However, unlike Σ_0 , the series terms in the expression for Σ_2 can only be found after the lengthy calculation.

Approximate solution

To avoid the long calculation to find the coefficients, a_1 to a_5 , a method of fitting the rational form

$$S = 1 + \frac{\vartheta t + (L_2 - 1)w_1 t^2}{1 + w_2 t + w_1 t^2}, \quad (4.75)$$

to the exact result is presented. At $t = 0$ this approximate form agrees with Σ_2 and its derivative. At the other extreme when $t \rightarrow \infty$, the approximate form S approaches the limit L_2 . The parameters w_1 and w_2 are adjusted to render a reasonable approximation and this is accomplished by interpolating the expression for S through two suitably chosen points $[t_1, S_1]$ and $[t_2, S_2]$. At these two interpolation points $S = \Sigma_2$. By trial and error, it has been found

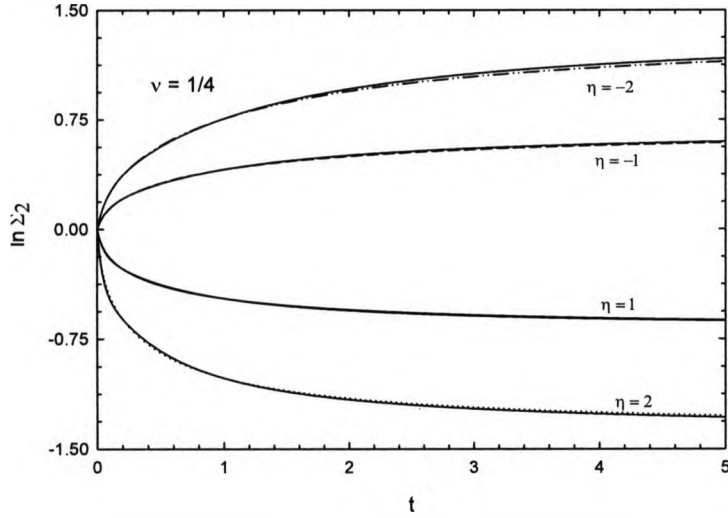


Figure 4.4: Graph of $\ln \Sigma_2$ versus t for the values of η shown and Poisson's ratio $\nu_0 = 1/4$. At $t = 0$ the slope is equal to ϑ which is given by equation (4.74). For large values of t the limiting values $\pm 11\eta/16$ are attained. The solid lines represent the series solution and the dashed lines are obtained from approximation given in equation (4.75)

that setting $t_1 = 1/5$ and $t_2 = 1$ produces an expression S with a relative error $(\Sigma_2 - S)/\Sigma_2 < 0.05$. After some algebra it is found that the parameter w_1 is

$$\begin{aligned} w_1 = & (1 - 2\nu_0)(1 - 4\nu_0) (14.55 \delta_0 + 28.83 \delta_1 + 8.354 \delta_{-1} + 69.64 \delta_2 + 5.486 \delta_{-2}) \\ & + 8\nu_0(1 - 2\nu_0) (12.92 \delta_0 + 27.45 \delta_1 + 6.816 \delta_{-1} + 72.44 \delta_2 + 3.986 \delta_{-2}) \\ & + 2\nu_0(4\nu_0 - 1) (11.00 \delta_0 + 25.30 \delta_1 + 5.453 \delta_{-1} + 73.87 \delta_2 + 2.989 \delta_{-2}), \end{aligned}$$

and w_2 is given by

$$\begin{aligned} w_2 = & (1 - 2\nu_0)(1 - 4\nu_0) (13.09 \delta_0 + 17.65 \delta_1 + 11.05 \delta_{-1} + 27.04 \delta_2 + 10.78 \delta_{-2}) \\ & + 8\nu_0(1 - 2\nu_0) (13.62 \delta_0 + 19.17 \delta_1 + 10.66 \delta_{-1} + 30.01 \delta_2 + 9.250 \delta_{-2}) \\ & + 2\nu_0(4\nu_0 - 1) (14.25 \delta_0 + 20.48 \delta_1 + 10.79 \delta_{-1} + 32.99 \delta_2 + 8.852 \delta_{-2}). \end{aligned}$$

The Lagrangian interpolation functions are,

$$\begin{aligned}
 \delta_0 &= (1 - \eta^2)(4 - \eta^2)/4, \\
 \delta_1 &= (1 + \eta)(4 - \eta^2)\eta/6, \\
 \delta_{-1} &= (\eta - 1)(4 - \eta^2)\eta/6, \\
 \delta_2 &= (\eta + 2)(\eta^2 - 1)\eta/24, \\
 \delta_{-2} &= (\eta - 2)(\eta^2 - 1)\eta/24.
 \end{aligned} \tag{4.76}$$

For example if $\nu_0 = 1/4$ and $\eta = 1$, then $L_2 \approx .5028$, $\vartheta \approx -4.282$, $w_1 \approx 27.45$, and $w_2 \approx 19.17$. The approximation S is then found to be

$$S = 1.0 + \frac{-4.282t - 13.65t^2}{1.0 + 19.17t + 27.45t^2},$$

and as shown in Fig. 4.4 this gives a reasonably accurate approximation.

4.6.3 Influence of varying Poisson's ratio upon K_0

The goal here is to find the effect of varying Poisson's ratio upon the stress concentration factors when Young's modulus is almost constant. Letting η approach zero corresponds to constant stiffness and it is desired that ν change from ν_1 to ν_∞ as the radius increases. Poisson's ratio is given in equation (4.2) and as $\eta \rightarrow 0$, the function $\kappa \approx 1 + \eta\rho^s$. Poisson's ratio is then given by $\nu = \nu_\infty + (\nu_1 - \nu_\infty)\rho^s$ and the coefficient ν_0 is given by

$$\nu_0 \approx \frac{\omega}{\eta}, \tag{4.77}$$

where $\omega = \nu_\infty - \nu_1$. Using equation (4.77) and as η approaches zero,

$$\Sigma_0 = \frac{1}{M(t(1 + \nu_0), 1 + 2t, \eta)} \rightarrow \frac{1}{{}_0F_1(1 + 2t, \omega t)}, \tag{4.78}$$

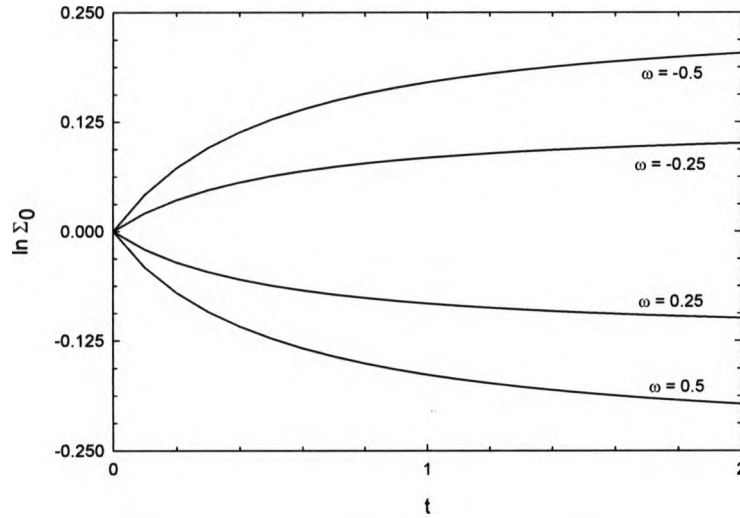


Figure 4.5: Graph of $\ln \Sigma_0$ versus t for the values of ω shown. The coefficient $\eta \rightarrow 0$ and Young's modulus is virtually constant; nonetheless, Poisson's ratio varies between ν_1 and ν_∞ . The stress concentration factor differs by 28% from the case where Poisson's ratio is constant

where ${}_0F_1(a, x)$ is the Hypergeometric function and some of its basic properties can be found in references [34, 35]. For the case of homogeneous materials, i.e. $\omega = 0$, the coefficient $\Sigma_0 = 1$ and $K_0 = 2$. Fig. 4.5 shows the distribution of $\ln \Sigma_0$ versus t for various values of ω . For the maximum change in Poisson's ratio, i.e. $|\omega| = 0.5$, it is found that as t becomes large K_0 changes by 28% from the case where Poisson's ratio is constant.

4.6.4 Influence of varying Poisson's ratio upon K_2

Considering $\eta \rightarrow 0$, performing the same limiting process, and using equation (4.77), the governing differential equation (4.40) for the case of almost constant Young's modulus is written as

$$\rho^4 f'''' + 2\rho^3 f''' - [9 - \omega s \rho^s] \rho^2 f''$$

$$\begin{aligned}
& + [9 + \omega s(s - 1)\rho^s] \rho f' \\
& + + [4\omega s(1 - s)\rho^s] f = 0.
\end{aligned} \tag{4.79}$$

As mentioned before, only three linearly independent solutions of equation (4.79) yield bounded stresses when $\rho \rightarrow \infty$ and they are written as

$$f_1(\rho) = \frac{\rho^2}{2} {}_2F_3 \left(\frac{1}{2} - t + \frac{\zeta}{2}, \frac{1}{2} - t - \frac{\zeta}{2}; 1 - 2t, 1 + 2t, 1 - 4t; \omega t \rho^s \right), \tag{4.80}$$

$$f_2(\rho) = \frac{1}{2\rho^2} {}_2F_3 \left(\frac{1}{2} + 3t + \frac{\zeta}{2}, \frac{1}{2} + 3t - \frac{\zeta}{2}; 1 + 4t, 1 + 2t, 1 + 6t; \omega t \rho^s \right) \tag{4.81}$$

$$f_3(\rho) = {}_2F_3 \left(\frac{1}{2} + t + \frac{\zeta}{2}, \frac{1}{2} + t - \frac{\zeta}{2}; 1 - 2t, 1 + 2t, 1 + 4t; \omega t \rho^s \right), \tag{4.82}$$

where the coefficient

$$\zeta = \sqrt{1 - 12t - 12t^2}, \tag{4.83}$$

and ${}_2F_3(a, b; c, d, e; x)$ is the Hypergeometric function; some of its basic properties can be found in references [34, 35]. Using equations (4.63) and (4.64), the normalized stress concentration factor Σ_2 is calculated. Fig. 4.6 shows the distribution of $\ln \Sigma_2$ versus t for different values of ω . For the case of homogeneous materials, i.e. $\omega = 0$, the coefficient $\Sigma_2 = 1$ and $K_2 = 4$. It is noted that for the maximum change in Poisson's ratio, as t becomes large K_2 changes by 13% from the case where Poisson's ratio is constant.

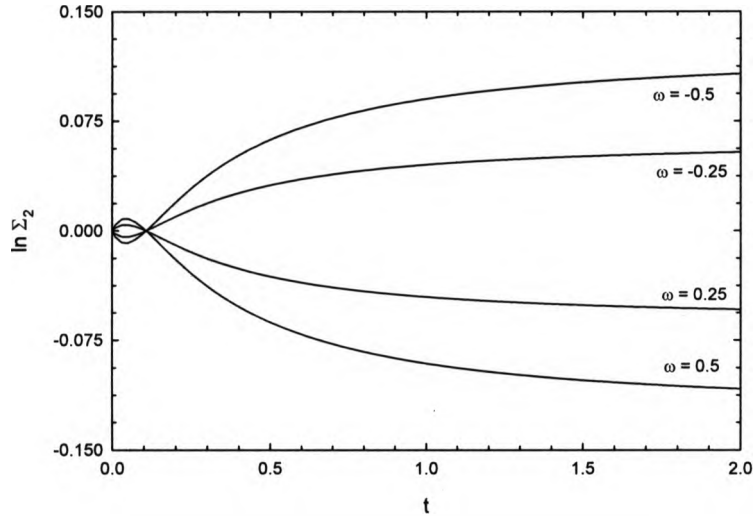


Figure 4.6: Graph of $\ln \Sigma_2$ versus t for the values of ω shown. The coefficient $\eta \rightarrow 0$ and Young's modulus is virtually constant; nonetheless, Poisson's ratio varies between ν_1 and ν_∞ . The stress concentration factor differs by 13% from the case where Poisson's ratio is constant

4.7 Concluding Remarks

In this paper the stress concentration factor around a circular hole in a radially inhomogeneous plate subjected to uniform biaxial tension and pure shear loading has been considered. An exponential function has been used to model the spatial variation of the elastic properties. The parameters η and s can be adjusted so that the shape of this function is reasonably general.

An analytical expression (4.31) for the stress concentration factor K_0 , i.e. uniform biaxial tension, was calculated. The normalized stress concentration factor Σ_0 was presented in terms of Kummer's function. The two Kummer's functions are given in equation (4.34). If $t = -1/s$, then it appears that the values $t = (1 + N)/2$ where N is an integer is not possible; otherwise the function $p_1(\rho)$ is not defined. However, because K_0 depends on the Wronskian, these forbidden values of t are not problematic. A similar phenomenon occurs

when K_2 is calculated.

Poisson's ratio is considered as constant and the effect of nonhomogeneous stiffness is considered on K_0 and K_2 . Since K_2 does not have a closed form solution, a reasonable approximation in the range $|\eta| < 2$ has been devised. Subsequently, Young's modulus was considered virtually constant and a limiting process was performed. It is concluded that for the maximum change in Poisson's ratio, as t becomes large K_0 and K_2 change by 28% and 13% respectively from the case where Poisson's ratio is constant.

Bibliography

- [1] M. Koizumi. FGM activities in Japan. *Composites Part B*, 28B:1–4, 1997.
- [2] F. Watari, A. Yokoyama, F. Saso, M. Uo, and T. Kawasaki. Fabrication and properties of functionally graded dental implant. *Composites Part B*, 28:pp. 5–11, 1997.
- [3] J. Simonet, G. Kapelski, and D. Bouvard. A sedimentation process for the fabrication of solid oxide fuel cell cathodes with graded composition. *Journal of the European Ceramic Society*, 27:3113–3116, 2007.
- [4] Y. Miyamoto, W.A. Kaysser, R.H. Rabin, A. Kawasaki, and R.G. Ford. *Functionally Graded Materials: Design, Processing and Applications*. Kluwer Academic Publishers, USA, 1999.
- [5] A.J. Markworth, K.S. Ramesh, and W.P. Parks. Modelling studies applied to functionally graded materials. *Journal of Materials Science*, 30:2183–2193, 1995.

- [6] Y. Watanabe and Y. Fukui. Fabrication of aluminum based functionally graded materials by centrifugal method and their physical properties. *Light Metals*, vol. 46:pp. 395–403, 1996.
- [7] M.U. Islam. An overview of research in the fields of laser surface modification and laser machining at the integrated manufacturing technologies institute NRC. *Advanced Performance Materials*, 3:215–238, 1996.
- [8] C.O. Horgan and A.M. Chan. The pressurized hollow cylinder or disk problem for functionally graded isotropic linearly elastic materials. *Journal of Elasticity*, 55:pp. 43–59, 1999.
- [9] N. Noda. Thermal stresses in functionally graded materials. *Journal of Thermal Stresses*, 22:477–512, 1999.
- [10] R.W. Zimmerman and M.P. Lutz. Thermal stresses and thermal expansion in a uniformly heated functionally graded cylinder. *Journal of Thermal Stresses*, 22:177–188, 1999.
- [11] J. Dryden and K. Jayaraman. Effect of inhomogeneity on the stress in pipes. *Journal Elasticity*, 83:179–189, 2006.
- [12] N. Tutuncu. Stresses in thick-walled FGM cylinders with exponentially-varying properties. *Engineering Structures*, 29:2032–2035, 2007.
- [13] M. Mohammadi and J.R. Dryden. Influence of the spatial variation of poisson's ratio upon the elastic field in nonhomogeneous axisymmetric bodies. *International Journal of Solids and Structures*, 46:225–232, 2009.
- [14] G.A. Kardomateas. Bending of a cylindrically orthotropic curved beam with linearly distributed elastic constants. *The Quarterly Journal of Mechanics and Applied Mathematics*, 43:43–56, 1990.

- [15] J.R. Dryden. Bending of inhomogeneous curved bars. *International Journal of Solids and Structures*, 44:4158–4166, 2007.
- [16] M. Mohammadi and J.R. Dryden. Thermal stresses in a nonhomogeneous curved beam. *Journal of Thermal Stresses*, 31:587–598, 2008.
- [17] M. Jabbari, S. Sohrabpour, and M.R. Eslami. Mechanical and thermal stresses in a functionally graded hollow cylinder due to radially symmetric loads. *International Journal of Pressure Vessels and Piping*, 79:493–497, 2002.
- [18] M.P. Lutz and R.W. Zimmerman. Thermal stresses and effective thermal expansion coefficient of a functionally gradient sphere. *Journal of Thermal Stresses*, 19:39–54, 1996.
- [19] G.J. Nie and R.C. Batra. Static deformations of functionally graded polar-orthotropic cylinders with elliptical inner and circular outer surfaces. *Composites Science and Technology*, doi:10.1016/j.compscitech.2009.11.018, 2009.
- [20] R.C. Batra and G.J. Nie. Analytical solutions for functionally graded incompressible eccentric and non-axisymmetrically loaded circular cylinders. *Composite Structures*, doi:10.1016/j.compstruct.2009.10.022, 2009.
- [21] S.G. Lekhnitskii. *Theory of Elasticity of an Anisotropic Body*. Mir Publishers, Moscow, 1981.
- [22] Z. S. Shao, K. K. Ang, J. N. Reddy, and T. J. Wang. Nonaxisymmetric thermomechanical analysis of functionally graded hollow cylinders. *Journal of Thermal Stresses*, 31:pp. 515–536, 2008.

- [23] R. Poultangari, M. Jabbari, and M.R. Eslami. Functionally graded hollow spheres under non-axisymmetric thermo-mechanical loads. *International Journal of Pressure Vessels and Piping*, 85:295–305, 2008.
- [24] M. Jabbari, S. Sohrabpour, and M.R. Eslami. General solutions for mechanical and thermal stresses in a functionally graded hollow cylinder due to nonaxisymmetric steady-state loads. *Journal of Applied Mechanics Transactions of ASME*, 70:pp. 111–118, 2003.
- [25] M.P. Lutz and R.W. Zimmerman. Effect of the interphase zone on the bulk modulus of a particulate composite. *Journal of Applied Mechanics Transactions of ASME*, 63:855–861, 1996.
- [26] G.N. Savin. *Stress Concentration around Holes*. International Series of Monographs in Aeronautics and Astronautics. Pergamon Press, New York, 1961.
- [27] W.D. Pilkey and D.F. Pilkey. *Peterson's Stress Concentration Factors*. John Wiley and Sons INC., Hoboken, New Jersey, third edition, 2008.
- [28] D.V. Kubair and B. Bhanu-Chandar. Stress concentration factor due to a circular hole in functionally graded panels under uniaxial tension. *International Journal of Mechanical Sciences*, 50:pp. 732–742, 2008.
- [29] Q. Yang, C.-F. Gao, and W. Chen. Stress analysis of a functional graded material plate with a circular hole. *Archive of Applied Mechanics*, July 2009.
- [30] S. Timoshenko and J.N. Goodier. *Theory of Elasticity*. McGraw-Hill, New York, third edition, 1970.

- [31] C. Wang. Applied Elasticity. McGraw-Hill, New York, 1953.
- [32] A.E.H. Love. A Treatise on the Mathematical Theory of Elasticity. Cambridge University Press Warehouse, second edition, 1906.
- [33] M. Braun. Differential Equations and Their Applications. Springer, New York, fourth edition, 1993.
- [34] M. Abramowitz and I.A. Stegun, editors. Handbook of Mathematical Functions. Dover Publications, INC., New York, 1972.
- [35] A. Erdelyi. Higher Transcendental Functions, volume vol. 1. Robert E. Krieger Publishing Company, Malabar, Florida, 1981.

Chapter 5

Conclusions and Future Work

In this thesis the elastic field in functionally graded materials has been considered and the conclusions are:

1. The thermal stress in a FG curved beam and a ring has been investigated. For the range of outer to inner radii examined here, i.e. $1 < b/a < 2$, good agreement has been observed between the analytical solution and the curved beam approximation.
2. The effect of varying Poisson's ratio on the elastic field in a ring has been considered. In the literature it is generally assumed that Poisson's ratio has an insignificant influence on the stress field. Here, it is found that the maximum hoop stress changes by up to $\pm 12\%$ when Poisson's ratio is considered to vary.
3. The stress concentration factor around a hole in a FG plate is considered, and for uniaxial tension, the stress concentration factor is written as

$$K = \frac{E_1}{E_\infty} (\Sigma_0 + 2\Sigma_2).$$

For the case of nonhomogeneous materials, $E_1 = E_\infty$ and $\Sigma_0 = \Sigma_2 = 1$ so that $K = 3$. For FGMs the ratio $E_1/E_\infty \neq 1$ and this accounts for the principal change in K .

For future work, the stress distribution around noncircular pipes is of interest. Also, for the purpose of design, the calculation of upper and lower bounds for stiffness would be a useful exercise.

Bibliography

- [1] M. Koizumi. FGM activities in Japan. *Composites Part B*, 28B:1–4, 1997.
- [2] C.O. Horgan and A.M. Chan. The pressurized hollow cylinder or disk problem for functionally graded isotropic linearly elastic materials. *Journal of Elasticity*, 55:pp. 43–59, 1999.
- [3] M. Jabbari, S. Sohrabpour, and M.R. Eslami. Mechanical and thermal stresses in a functionally graded hollow cylinder due to radially symmetric loads. *International Journal of Pressure Vessels and Piping*, 79:493–497, 2002.
- [4] V. Birman and L.W. Byrd. Modeling and analysis of functionally graded materials and structure. *Applied Mechanics Reviews*, 60:195–216, 2007.
- [5] F. Watari, A. Yokoyama, F. Saso, M. Uo, and T. Kawasaki. Fabrication and properties of functionally graded dental implant. *Composites Part B*, 28:pp. 5–11, 1997.
- [6] J. Simonet, G. Kapelski, and D. Bouvard. A sedimentation process for the fabrication of solid oxide fuel cell cathodes with graded composition. *Journal of the European Ceramic Society*, 27:3113–3116, 2007.
- [7] E. Muller, C. Draar, J. Schilz, and W.A. Kaysser. Functionally graded materials for sensor and energy applications. *Materials Science and Engineering A*, 362:17–39, 2003.
- [8] Y. Miyamoto, W.A. Kaysser, R.H. Rabin, A. Kawasaki, and R.G. Ford. *Functionally Graded Materials: Design, Processing and Applications*. Kluwer Academic Publishers, USA, 1999.
- [9] A.J. Markworth, K.S. Ramesh, and W.P. Parks. Modelling studies applied to functionally graded materials. *Journal of Materials Science*, 30:2183–2193, 1995.
- [10] Y. Fukui, N. Yamanaka, and K. Wakashima. The stresses and strains in a thick-walled tube for functionally graded material under uniform thermal loading. *JSME International Journal A-Solid Mechanic*, 36:156–162, 1993.
- [11] G. Subbaraman and K.L. Reifsnider. Mechanical response of fuel clad with radial property variations. In *12th Annual. Mtg. Ses.*, volume 36, pages 1235–1247, University of Texas, 1976.

- [12] L.B. Freund and S. Suresh. *Thin Film Materials*. Cambridge University Press, Cambridge, 2003.
- [13] M. Picasso, C.F. Marsden, J.D. Wagniere, A. Frenk, and M. Rappaz. A simple but realistic model for laser cladding. *Metallurgical and Materials Transactions B*, 25:281–291, 1994.
- [14] M.U. Islam. An overview of research in the fields of laser surface modification and laser machining at the integrated manufacturing technologies institute NRC. *Advanced Performance Materials*, 3:215–238, 1996.
- [15] M.S. Ozmusul and R.C. Picu. Elastic moduli of particulate composites with graded filler-matrix interface. *Polymer Composites*, 23:110–119, 2002.
- [16] S.G. Lekhnitskii. *Theory of Elasticity of an Anisotropic Body*. Mir Publishers, Moscow, 1981.
- [17] N. Noda. Thermal stresses in functionally graded materials. *Journal of Thermal Stresses*, 22:477–512, 1999.
- [18] N. Tutuncu and M. Ozturk. Exact solutions for stresses in functionally graded pressure vessels. *Composites Part B: Engineering*, 32:493–497, 2001.
- [19] G.A. Kardomateas. Bending of a cylindrically orthotropic curved beam with linearly distributed elastic constants. *The Quarterly Journal of Mechanics and Applied Mathematics*, 43:43–56, 1990.
- [20] J.R. Dryden. Bending of inhomogeneous curved bars. *International Journal of Solids and Structures*, 44:4158–4166, 2007.
- [21] B.A. Boley and E.S. Barrekette. Thermal stress in curved beams. *J. Aero. Space. Sci.*, 25:627–630, p. 643, 1958.
- [22] D. Iesan. On the thermal stresses in beams. *J. Eng. Math.*, 6:155–163, 1972.
- [23] S. Chirita. Thermal stresses in anisotropic cylinders. *Acta Mech.*, vol. 23:301–306, 1975.
- [24] D. Iesan. Thermal stresses in composite cylinders. *J. Therm. Stresses*, 3:495–508, 1980.

- [25] S. Chirita. Thermal stresses in anisotropic noncylindrical beams. *Rev. Roum. Sci. Techn-Mec. Appl.*, 28:63–74, 1983.
- [26] M. Mohammadi and J.R. Dryden. Thermal stress in a functionally graded curved bar. In *The Proceedings of Simulation and Modeling (MS 2007)*, pages 250–253, Montreal, Quebec, Canada, 2007.
- [27] P.R. Marur and H.V. Tippur. Evaluation of mechanical properties of functionally graded materials. *Journal of Testing and Evaluation*, 26:539–545, 1998.
- [28] R.W. Zimmerman and M.P. Lutz. Thermal stresses and thermal expansion in a uniformly heated functionally graded cylinder. *Journal of Thermal Stresses*, 22:177–188, 1999.
- [29] M.P. Lutz and R.W. Zimmerman. Thermal stresses and effective thermal expansion coefficient of a functionally gradient sphere. *Journal of Thermal Stresses*, 19:39–54, 1996.
- [30] G.H. Paulino and J-H. Kim. On the poisson's ratio effect on mixed-mode stress intensity factors and t-stress in functionally graded materials. *International Journal of Computational Engineering Science*, 5:833–861, 2004.
- [31] A.N. Eraslan. Stresses in FGM pressure tubes under non-uniform temperature distribution. *Structural Engineering and Mechanics*, 26:393–408, 2006.
- [32] G.J. Nie and R.C. Batra. Static deformations of functionally graded polar-orthotropic cylinders with elliptical inner and circular outer surfaces. *Composites Science and Technology*, doi:10.1016/j.compscitech.2009.11.018, 2009.
- [33] R.C. Batra and G.J. Nie. Analytical solutions for functionally graded incompressible eccentric and non-axisymmetrically loaded circular cylinders. *Composite Structures*, doi:10.1016/j.compstruct.2009.10.022, 2009.
- [34] Z. S. Shao, K. K. Ang, J. N. Reddy, and T. J. Wang. Nonaxisymmetric thermomechanical analysis of functionally graded hollow cylinders. *Journal of Thermal Stresses*, 31:pp. 515–536, 2008.
- [35] R. Poultangari, M. Jabbari, and M.R. Eslami. Functionally graded hollow spheres under non-axisymmetric thermo-mechanical loads. *International Journal of Pressure Vessels and Piping*, 85:295–305, 2008.

- [36] M. Jabbari, S. Sohrabpour, and M.R. Eslami. General solutions for mechanical and thermal stresses in a functionally graded hollow cylinder due to nonaxisymmetric steady-state loads. *Journal of Applied Mechanics Transactions of ASME*, 70:pp. 111–118, 2003.
- [37] M.P. Lutz and R.W. Zimmerman. Effect of the interphase zone on the bulk modulus of a particulate composite. *Journal of Applied Mechanics Transactions of ASME*, 63:855–861, 1996.
- [38] G.N. Savin. *Stress Concentration around Holes*. International Series of Monographs in Aeronautics and Astronautics. Pergamon Press, New York, 1961.
- [39] W.D. Pilkey and D.F. Pilkey. *Peterson's Stress Concentration Factors*. John Wiley and Sons INC., Hoboken, New Jersey, third edition, 2008.
- [40] D.V. Kubair and B. Bhanu-Chandar. Stress concentration factor due to a circular hole in functionally graded panels under uniaxial tension. *International Journal of Mechanical Sciences*, 50:pp. 732–742, 2008.
- [41] Q. Yang, C.-F. Gao, and W. Chen. Stress analysis of a functional graded material plate with a circular hole. *Archive of Applied Mechanics*, July 2009.
- [42] B. Paul. Prediction of elastic constants of multiphase materials. *Transactions of the Metallurgical Society-AIME*, 218:36–41, 1960.
- [43] Y. Watanabe and Y. Fukui. Fabrication of aluminum based functionally graded materials by centrifugal method and their physical properties. *Light Metals*, vol. 46:pp. 395–403, 1996.
- [44] A.E.H. Love. *A Treatise on the Mathematical Theory of Elasticity*. Cambridge University Press Warehouse, second edition, 1906.
- [45] S. Timoshenko and J.N. Goodier. *Theory of Elasticity*. McGraw-Hill, New York, third edition, 1970.
- [46] B.A. Boley and J.H. Weiner. *Theory of Thermal Stresses*. Dover Publication, INC., Mineola, New York, 1997.
- [47] Y.A. Amenzadeh. *Theory of Elasticity*. Mir Publishers, Moscow, 1979.
- [48] F.B. Hildebrand. *Methods of Applied Mathematics*. Dover Publication, INC., Mineola, New York, second edition, 1965.

- [49] E. Zauderer. *Partial Differential Equations of Applied Mathematics*. John Wiley and Sons, Inc., Hoboken, New Jersey, third edition, 2006.
- [50] J. Dryden and K. Jayaraman. Effect of inhomogeneity on the stress in pipes. *Journal Elasticity*, 83:179–189, 2006.
- [51] M. Abramowitz and I.A. Stegun, editors. *Handbook of Mathematical Functions*. Dover Publications, INC., New York, 1972.
- [52] W.W. Bell. *Special Functions for Scientists and Engineers*. D. Van Nostrand Company Ltd., London, 1968.
- [53] M. Ashby. *Materials Selection in Mechanical Design*. Butterworth and Heine, Oxford, 1999.
- [54] M. Sasaki and T. Hirai. Fabrication and properties of functionally gradient materials. *Journal of the Ceramic Society of Japan*, 99:1002–1013, 1991.
- [55] M. Mohammadi and J.R. Dryden. Thermal stresses in a nonhomogeneous curved beam. *Journal of Thermal Stresses*, 31:587–598, 2008.
- [56] M. Braun. *Differential Equations and Their Applications*. Springer, New York, fourth edition, 1993.
- [57] N. Tutuncu. Stresses in thick-walled FGM cylinders with exponentially-varying properties. *Engineering Structures*, 29:2032–2035, 2007.
- [58] M. Mohammadi and J.R. Dryden. Influence of the spatial variation of poisson's ratio upon the elastic field in nonhomogeneous axisymmetric bodies. *International Journal of Solids and Structures*, 46:225–232, 2009.
- [59] C. Wang. *Applied Elasticity*. McGraw-Hill, New York, 1953.
- [60] A. Erdelyi. *Higher Transcendental Functions*, volume vol. 1. Robert E. Krieger Publishing Company, Malabar, Florida, 1981.